minerals

MDPI

Article

Evolution of Nb–Ta Oxide Minerals and Their Relationship to the Magmatic-Hydrothermal Processes of the Nb–Ta Mineralized Syenitic Dikes in the Panxi Region, SW China

Yuan Xue [1,2], Ningyue Sun [1] and Guowu Li [1,*]

[1] Crystal Structure Laboratory, Science Research Institute, China University of Geosciences (Beijing), Beijing 100083, China; 2019600003@cugb.edu.cn (Y.X.); sunningyue1998@163.com (N.S.)
[2] School of Materials Science and Technology, China University of Geosciences (Beijing), Beijing 100083, China
* Correspondence: liguowu@cugb.edu.cn; Tel.: +86-010-8232-2243

Abstract: Previous geochemical and petrological studies have concluded that initially magmatic Nb–Ta mineralization is often modified by post-magmatic hydrothermal fluids; however, there is still a lack of mineralogical evidence for the syenite-related Nb–Ta deposit. From the perspective of Nb–Ta minerals, the pyrochlore supergroup minerals have significance for indicating the fluid evolution of alkaline rock or related carbonatite type Nb–Ta deposits. The Panzhihua–Xichang (Panxi) region is a famous polymetallic metallogenic belt in southwestern China, abound with a huge amount of Nb–Ta mineralized syenitic dikes. This study focuses on the mineral textures and chemical compositions of the main Nb–Ta oxide minerals (including columbite-(Fe), fersmite, fergusonite-(Y), and especially pyrochlore group minerals) in samples from the Baicao and Xiaoheiqing deposits, in the Huili area, Panxi region, to reveal the magma evolution process of syenitic-dike-related Nb–Ta deposits. The Nb–Ta oxides in the Huili syenites are commonly characterized by a specific two-stage texture on the crystal scale, exhibiting a complex metasomatic structure and compositional zoning. Four types of pyrochlore group minerals (pyrochlores I, II, III, and IV) formed in different stages were identified. The euhedral columbite-(Fe), fersmite, and pyrochlores I and II minerals formed in the magmatic fractional crystallization stage. Anhedral pyrochlore III minerals are linked to the activity of magma-derived hydrothermal fluids at the late stages of magma evolution. The pyrochlore IV minerals and fergusonite-(Y) tend to be more concentrated in areas that have undergone strong albitization, which is a typical phenomenon of hydrothermal alteration. These mineralogical phenomena provide strong evidences that the magmatic-hydrothermal transitional stage is the favored model for explaining the Nb–Ta mineralization process. It is also concluded that the changes in chemical composition and texture characteristics for pyrochlore group minerals could serve as a proxy for syenite-related Nb–Ta mineralization processes.

Keywords: Nb–Ta mineralization; syenitic dike; Panxi region; pyrochlore group minerals; columbite subgroup minerals

Citation: Xue, Y.; Sun, N.; Li, G. Evolution of Nb–Ta Oxide Minerals and Their Relationship to the Magmatic-Hydrothermal Processes of the Nb–Ta Mineralized Syenitic Dikes in the Panxi Region, SW China. *Minerals* **2021**, *11*, 1204. https://doi.org/10.3390/min11111204

Academic Editor: Daniel Atencio

Received: 25 September 2021
Accepted: 26 October 2021
Published: 29 October 2021

1. Introduction

Most economically significant magmatic Nb deposits are associated with either carbonatites or felsic igneous rocks [1]. Carbonatite is reserved for igneous rocks containing 50% or more of modal carbonate (typically, calcite, dolomite, ankerite, or siderite). In rare-metal deposits of carbonatite, Nb is more common than Ta, and they usually have a deep affinity with REE or Zr [2,3]. Felsic igneous rocks include nepheline syenites, A-type granites and syenites [4–6], and related pegmatites [7–9]. In recent decades, two main views on the enrichment mechanism of magmatic Nb–Ta deposits have been developed. One view holds that Nb–Ta mineralization is the product of magmatic crystallization processes. This view is based on experimental data [9–12] and natural samples [13–18], which have shown that the enrichment of rare elements occurs during the fractionation of granitic melts. The

second view considers the fact that mineral metasomatism and alteration are common in some Nb–Ta deposits, suggesting that the enrichment of Nb–Ta deposits may be related to hydrothermal metasomatism [19–21]. To decipher the specific roles of magmatic and hydrothermal processes in the formation of magmatic rare element deposits, scholars conducted a series of mineralogical studies [22–30]. The veinlets of tantalite-(Fe) in the Nanping pegmatite in southern China [25] may indicate hydrothermal overprinting of magmatic rare element mineralization. The generation of rare element minerals in the Songshugang granite [27] demonstrate that a magmatic-hydrothermal transitional stage is a favored model for explaining the late-stage rare element mineralization. By means of piston cylinder experiments, Anenburg et al. [28] discussed the enrichment of rare metals in the last stages of magmatic fractionation in alkaline silica undersaturated systems. Therefore, rare element mineralization occurs during both magmatic and hydrothermal stages in peraluminous granites, alkaline granites, and pegmatites. However, only a few studies specialized in the Nb–Ta-bearing minerals in syenite system.

In this study, we focused on the mineral textures and chemical compositions of the main Nb–Ta oxide minerals (including columbite-(Fe), fersmite, fergusonite-(Y), and pyrochlore group minerals) in the syenitic dikes in Baicao and Xiaoheiqing deposits, Panzhihua–Xichang district, southwestern China, with the aim to track Nb–Ta mineralization. These mineral species and composition variations allowed for characterizing both the magmatic and hydrothermal crystallization stages. Our study showed that pyrochlore group minerals formed during almost the whole mineralization processes. Moreover, according to the new classification scheme for the pyrochlore supergroup minerals approved by the IMA-CNMNC in 2010 [31], pyrochlore supergroup minerals are defined as complex oxides with the general formula $A_{2-m}B_2X_{6-w}Y_{1-n}$ (m = 0–1.7, w = 0–0.7, n = 0–1.0). In this structure, there are four types of ion occupancies (Figure 1). The *A*-site can host cations such as Na^+, Ca^{2+}, Th^{4+}, U^{4+}, and REE^{3+}; the *B*-site can contain cations such as Nb^{5+}, Ta^{5+}, Ti^{4+}, Si^{4+}, and P^{5+}; the *X*-site typically contains O^{2-}; and the *Y*-site typically contains OH^-, F^-, O^{2-}, H_2O, etc. [31]. Thus, pyrochlore supergroup minerals are natural trackers and recorders of Na, Ca, REE, Nb, and Ta for indicating their content changes in melts or fluids, and of OH^- and F^- for indicating the volatile changes in the metallogenic environment, both of which have been proven to decipher details of the magmatic and hydrothermal processes in carbonatitic systems [32,33].

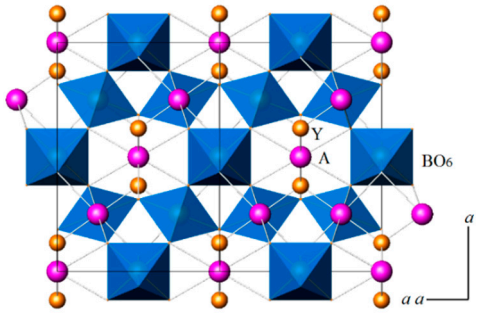

Figure 1. Schematic diagram of the crystal structure of the pyrochlore supergroup minerals.

The goals of this study were to: (i) describe the diversity of the individual Nb–Ta-containing minerals and their chemical compositions throughout the magmatic and hydrothermal crystallization stages; and (ii) discuss the controlling effects of the primary magmatic and post-magmatic hydrothermal volatiles on the composition of pyrochlore group minerals. This information provides insight into the hydrothermal Nb/Ta mineralization involved in syenite fractionation.

2. Geological Setting

The Panxi region (SW China) is located in the inner zone of the Emeishan large igneous province (ELIP) on the western margin of the Yangtze Block (Figure 2) [34]. This area is one

of China's historically important mineral resource areas, containing rare earth elements (REEs), Nb, Ta, Ti, and V relating to magmatic rocks. In this region, several N–S-trending faults have exposed numerous mafic–ultramafic intrusions that form a mineralized zone about 200 km long and 10–30 km wide [35]. These widely distributed mafic–ultramafic layered intrusions, flood basalts, and related felsic intrusions are considered to be important components of the ELIP [36] and are thought to have formed from magmas generated by a mantle plume [37].

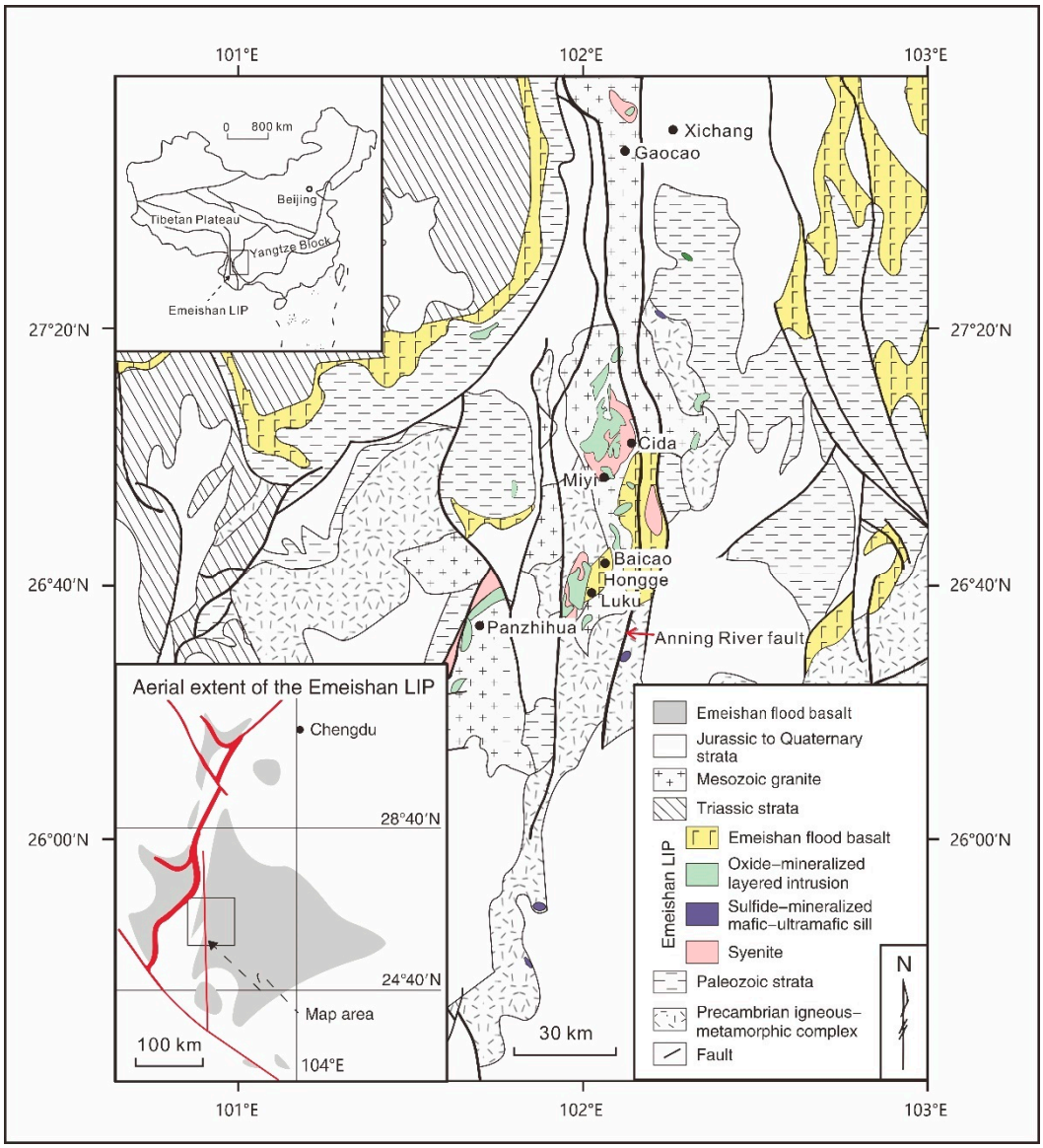

Figure 2. Geologic map of the Panxi region. Modified after [38–40].

Since the 1960s, more than 30 small Nb–Ta deposits have been reported in the Panxi region, and most of them are hosted in alkaline dikes [38]. Based on field mapping and analysis, several scholars have concluded that the Nb–Ta mineralized alkaline dikes are closely temporally and spatially related to the ELIP [41,42]. Previous studies have shown that the ELIP is related to Indosinian mantle plume activity [37,41,43–47]. As it is difficult to directly determine the age of mafic rocks, the age of the ELIP was determined based on the U–Pb zircon ages of related felsic intrusions, which are concentrated at 260–252 Ma, with a peak at ~260 Ma [42]. Moreover, the age of the Nb–Ta-bearing dikes is very close to the age of the ELIP. For example, the Cida mineralized alkaline rocks are 261 Ma (zircon

SHRIMP U–Pb dating; [41]). Therefore, the Nb–Ta metallogenic event is considered the product of Emeishan mantle plume activity [41,42].

Nevertheless, such an occurrence of Nb–Ta mineralization is rare in other LIPs [48,49]. The genetic relationship between the hydrothermal fluids and the Nb–Ta enrichment of these syenitic dikes is not clear. Previous research on the syenite type Nb–Ta deposit in the Panxi region have focused on its mineralization mechanism. Furthermore, several geochemical and petrological studies have determined that the Nb–Ta mineralization and enrichment in the Panxi region are controlled by magmatic fractional crystallization or post-magmatic hydrothermal metasomatism [38,50]. The Nb–Ta-dominant oxide minerals from the Panxi alkaline rocks have been described, but little attention has been paid to the association and paragenetic relationship of the Nb–Ta minerals and the mineralogical evidence of the mineral evolution.

Our study focuses on the Huili area on the western side of the Anning River fault, including the Baicao and Xiaoheiqing deposits (Figures 2 and 3). The Nb–Ta-bearing dikes in this area are mainly composed of syenites and alkaline pegmatites (258–256 Ma zircon U–Pb dating), occur in the eastern part of the syenitic plutons, and intrude into the mafic–ultramafic layered intrusions [38,51,52]. Three hundred and ten dikes have been found in the mining area, of which 73 veins are generally 100–300 m long (up to 1000 m long), 1–5 m in width, and 50–100 m in depth [53]. They are mainly alkalic dikes, including arfvedsonite syenite dikes, aegirine pegmatite syenite dikes, and granite pegmatite dikes.

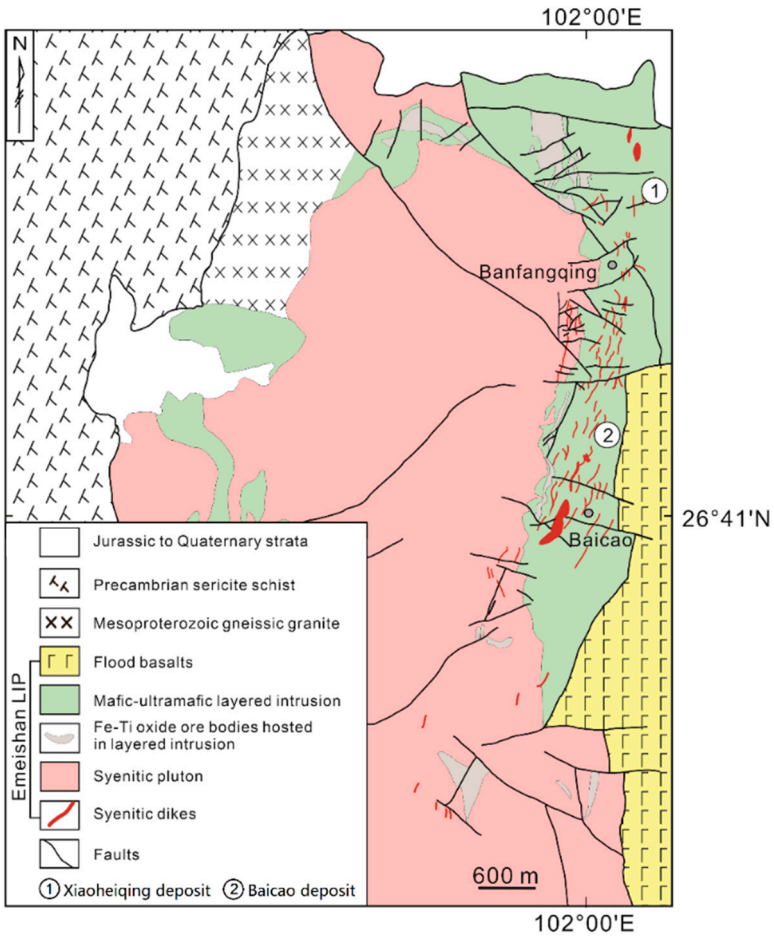

Figure 3. Simplified geologic map showing the syenitic dikes and syenitic pluton in the Baicao and Xiaoheiqing deposits. Modified after [54,55].

3. Petrography

The Nb–Ta mineralized dikes in the Huili area are composed of Indosinian alkaline syenite and alkaline pegmatite; they penetrate along the structural fissures in the Hercynian mafic–ultramafic layered intrusions (mainly gabbro) (Figure 4). This layered rock mass is the northern extension of the Hongge ferric-titanium-vanadium mafic–ultramafic rocks [56].

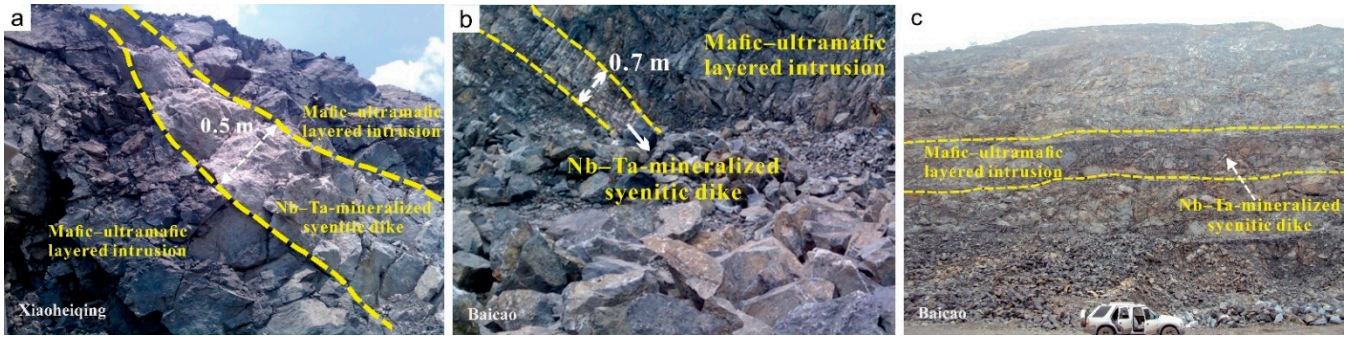

Figure 4. Field photos of the gray and white Nb–Ta mineralized syenitic dikes intruding the deep gray mafic–ultramafic layered intrusions: (**a**) sample point in Xiaoheiqing deposit (26°42′53.69″ N, 102°0′35.33″ E); (**b**) sample point in Baicao deposit (26°41′19.43″ N, 102°0′28.46″ E); and (**c**) large outcrop in Baicao deposit showing obvious layered intrusions and massive dike intrusions.

3.1. Mafic–Ultramafic Layered Intrusions

The main part of the mafic–ultramafic layered intrusions in the Huili area is composed of gabbro. The gabbro is deep gray with a medium grained texture and consists of Fe–Ti oxide minerals (20–28%), clinopyroxene (30–45%), and plagioclase (25–37%).

3.2. Nb–Ta Mineralized Syenitic Dikes

The rocks of the Nb–Ta mineralized syenitic dikes are gray and white with medium- to coarse-grained, subhedral granular, and metasomatic relict textures and a massive structure. The main minerals are K-feldspar (50–60%), albite (10–20%), aegirine (5–10%), and arfvedsonite (5–10%, partly biotitization). Parts of the K-feldspar phenocrysts have been replaced by albite and clay minerals, forming a metasomatic relict structure. Among them, the K-feldspar crystals are 1.0 mm × 0.8 mm to 22.3 mm × 9.0 mm tabular grains, and mainly composed of orthoclase with Carlsbad twinning, microcline, and perthite. The albite crystals are 0.1 mm to 1.3 mm tabular grains, and they often replace the margins of the coarse-grained K-feldspar crystals. The arfvedsonite crystals are 0.1–1.8 mm in size, green, and columnar, and they account for about 10% of the total minerals. Partial biotitization has resulted in a residual metasomatic structure. The total amount of accessory minerals is less than 5%. The accessory minerals include fluorite, titanite, thorite, zircon, allanite, chevkinite, epidote, clinozoisite, fluorapatite, monazite-(Ce), bastnäsite, baryte, pyrochlore, fergusonite, ilmenite, pyrophanite, magnetite, baddeleyite, zirconolite, bismoclite, galena, pyrite, and sphalerite.

Pyrochlore group minerals and fergusonite-(Y) are the major Nb–Ta-bearing minerals, which are described in detail in the mineralogy section.

4. Materials and Methods

Eighteen samples were obtained from the Nb–Ta mineralized syenitic dikes in the Baicao and Xiaoheiqing deposits. In addition to observations of petrographic thin sections under an optical microscope, accessory minerals were selected from the artificial heavy concentrate and were made into polished wafers for backscattered electron (BSE) observation and compositional analysis.

The chemical homogeneity, microstructural features, and mineral inclusions of the Nb–Ta oxide minerals were studied using a MIRA3 XMU field emission scanning electron microscope (SEM) in BSE mode and an Oxford X-MAX energy dispersive spectrometry (EDS) analyzer at the China University of Geosciences (Beijing), China, to survey the paragenetic assemblages and textures of the samples.

The chemical compositions were obtained using the JEOL JXA-8100 electron microprobe at the Beijing Research Institute of Uranium Geology, China. The minerals were analyzed in the wavelength-dispersive mode under the following operating conditions: 20 kV, 10 nA, and an electron beam diameter of 2 μm. Analytical standards were: Fluorapatite (F); Synth-$CaSiO_3$ (Ca); Albite (Na); Pyrope (Mg); Synth-YP_5O_{14} (Y); Synth-ThO_2 (Th); Synth-PrP_5O_{14} (Pr); Willemite (Si); Rutile (Ti); Synth-$KNbO_3$ (Nb); Tantalite-(Mn) (Ta); K-feldspar (Al); Synth-$MnSiO_3$ (Mn); Synth-$PbCrO_4$ (Pb); Monazite (Ce, La, Nd); and Metallic Fe and U (Fe, U).

Due to the complexity of the chemical compositions of the Nb–Ta minerals and the similarities between the compositional characteristics of the different mineral species, a single crystal diffractometer was used to conduct the X-ray diffraction analyses of the selected mineral particles to accurately identify the mineral species. The X-ray powder diffraction and single crystal diffraction data were acquired using the Rigaku Oxford diffraction XtaLAB PRO-007HF rotating anode microfocus X-ray source (50 kV, 24 mA, 1.2 kW, Mo$K\alpha$) with a hybrid pixel array detector and a single-crystal diffractometer at the China University of Geosciences (Beijing), China.

5. Results

5.1. Columbite-(Fe)

The columbite subgroup minerals are some of the most important Nb–Ta minerals in rare metal granite and granite pegmatite as their compositional characteristics and zoned structures serve as good tracers of the crystallization evolution process of these rocks [23,25,27,28,51,57–59]. However, in the Nb–Ta-bearing syenitic dikes in the Huili area, the columbite subgroup minerals are relatively rare and were only found in three samples from the Baicao deposit. As is shown in the BSE images, the columbite-(Fe) forms anhedral to subhedral crystals, which are disseminated in albite, biotite, and calcite, are intergrown with fersmite, and are up to 100 μm in diameter (Figure 5a,b). The columbite-(Fe) usually occurs as subhedral particles associated with ilmenite (Figure 5c), is wrapped by subhedral–anhedral zircon (Figure 5d), or is incompletely replaced by fluorcalciopyrochlore (Figure 5d–f), ranging from 50–100 μm in diameter.

The columbite-(Fe) is composed of 9.48–28.96 wt% FeO, 0.00–8.80 wt% MnO, 0.00–1.24 wt% TiO_2, 65.06–77.45 wt% Nb_2O_5, and 3.76–6.57 wt% Ta_2O_5, with Ta/(Nb + Ta) ratios of 0.03–0.05. Nine compositional data for columbite-(Fe) in the different samples from this area are plotted in Figure 6. The columbite subgroup minerals in the Huili syenitic dikes are all distributed in the Nb end-member of the columbite-(Fe) zone. The formula for the columbite-(Fe) calculated using a total of six oxygen atoms is $(Fe_{0.50}Mn_{0.43}Ti_{0.05})_{\sum 0.98}(Nb_{1.89}Ta_{0.10})_{\sum 1.99}O_6$.

Chemical analysis was conducted on the intergrown grains composed of disseminated columbite-(Fe) and fersmite. The results show that the Nb and Ta are evenly distributed, and the columbite-(Fe) grains have Ta/(Ta + Nb) atomic ratios (approximately 0.03–0.05) similar to those of the fersmite.

As is shown in Figure 5d–f, the rims of the anhedral columbite-(Fe) were replaced by fluorcalciopyrochlore, forming bright rims or bright veins along the fissures. This is the characteristic of typical replacement structural zoning. The map scanning results of this type of grain show that the (Fe, Mn, and Nb) and (Ca, Na, Ta, and Ti) element groups are similarly distributed, and the two groups exhibit reverse distributions. The point analysis results show that the Ta/(Ta + Nb) atomic ratios of the columbite-(Fe) and calciopyrochlore (Figure 5f) are 0.04 and 0.18, respectively.

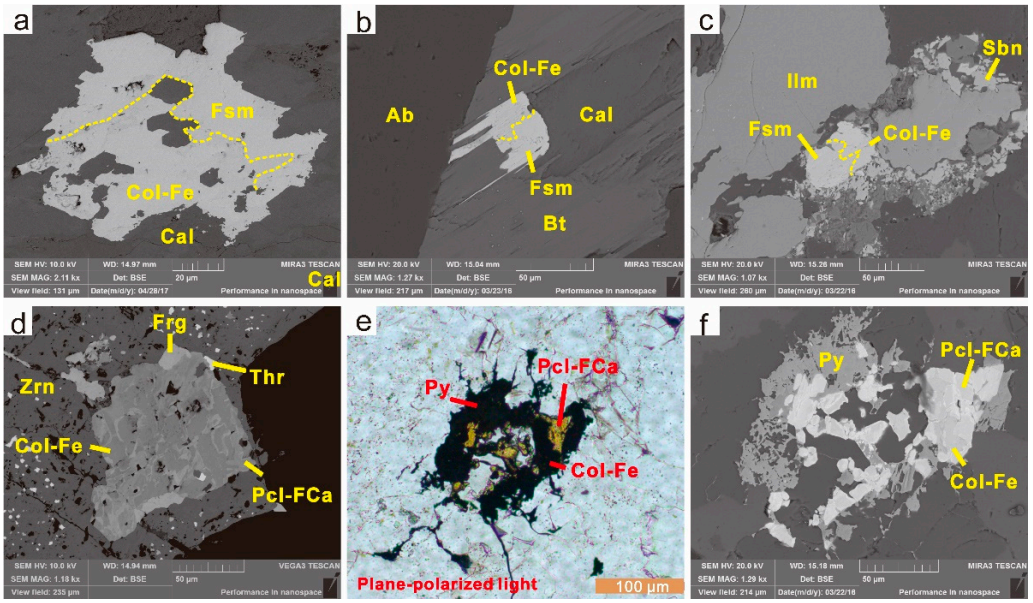

Figure 5. Photomicrographs and back-scattered electron (BSE) images of columbite-(Fe) with associated minerals. (**a**–**c**) Intergrown particles of columbite-(Fe) and fersmite (BSE); (**d**) Intergrown particles of columbite-(Fe) and fluorcalciopyrochlore (BSE); (**e**) photomicrographs of an incomplete pseudmorph of columbite-(Fe) replaced by fluorcalciopyrochlore; and (**f**) incomplete pseudomorph of columbite replaced by fluorcalciopyrochlore (BSE). Abbreviations: Ab—albite; Bt—biotite; Frg—fergusonite-(Y); Fsm—fersmite; Ilm—ilmenite; Col-Fe—columbite-(Fe); Pcl-FCa—fluorcalciopyrochlore; Py—pyrite; Sbn—sanbornite; Thr—thorite; and Zrn—zircon.

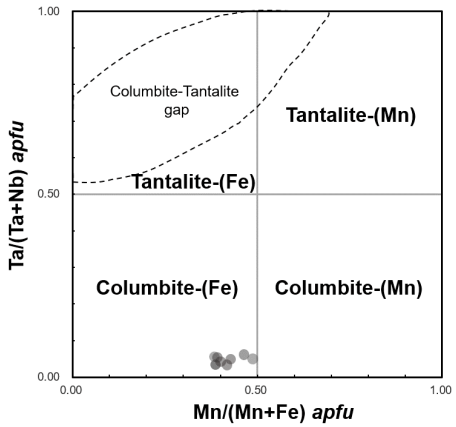

Figure 6. Compositional diagrams (atomic proportion) for the columbite-(Fe) from the Baicao and Xiaoheiqing deposits.

5.2. Fersmite

Fersmite is also a member of the columbite subgroup. It was found in individual syenite samples from Baicao deposit. Occasionally, the fersmite in the syenitic dikes occurs as euhedral crystals with uniformly distributed chemical compositions (Figure 7a,b). It occurs as anhedral grains and is mainly distributed among the rock-forming minerals, such as hedenbergite and K-feldspar (Figure 7c,d), but it is occasionally wrapped by subhedral fergusonite-(Y) (Figure 7d) or intergrown with columbite-(Fe) (Figure 5a,c). The fersmite in the syenitic dikes is closely related to the fluorcalciopyrochlore and is replaced by fluorcalciopyrochlore, forming bright rims (Figure 7e,f).

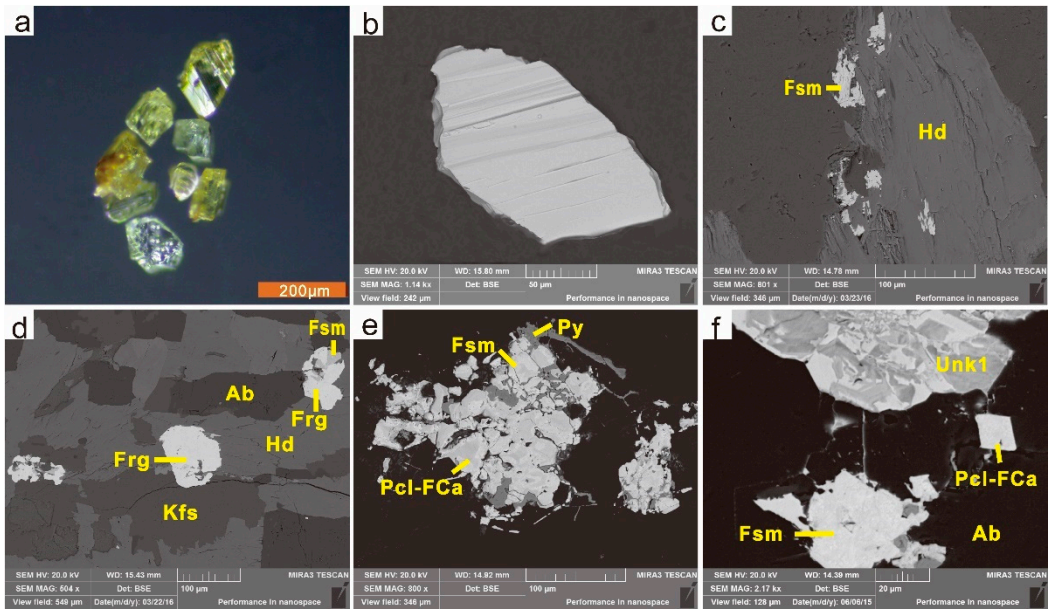

Figure 7. Photomicrographs and BSE images of fersmite with associated minerals. (**a**) Fersmite crystals; (**b**) a fersmite crystal (BSE) showing uniform composition distribution; (**c**) anhedral fersmite (BSE) distributed around hedenbergite; (**d**) subhedral fersmite associated with fergusonite-(Y) (BSE); (**e**) fersmite partly replaced by fluorcalciopyrochlore (BSE); and (**f**) an irregular aggregate of fersmite associated with fluorcalciopyrochlore (BSE). Abbreviations: Ab—albite; Frg—fergusonite-(Y); Fsm—fersmite; Hd—hedenbergite; Kfs—K-feldspar; Pcl-FCa—fluorcalciopyrochlore; Py—pyrite; Unk1—unknown mineral 1; and Zrn—zircon.

The euhedral fersmite is composed of 16.90–17.96 wt% CaO, 74.69–78.42 wt% Nb_2O_5, 0.09–0.95 wt% Ta_2O_5, 0.72–1.59 wt% TiO_2, and 1.64–3.28 wt% $\sum REE_2O_3$, with Ta/(Nb + Ta) ratios of 0.03–0.06. It is locally enriched in Y and is slightly enriched in Nd, Ce, and La. Its empirical formula, which was calculated based on six anions, is $(Ca_{1.01}Y_{0.06}Nd_{0.01})_{\sum 1.08}(Nb_{1.87}Ti_{0.05}Fe_{0.05}Ta_{0.01}Si_{0.01})_{\sum 2.00}O_{6.00}$.

5.3. Fergusonite-(Y)

Fergusonite-(Y) occurs as an accessory mineral and is widely dispersed in the Baicao and Xiaoheiqing Nb–Ta deposits. The fergusonite-(Y) exhibits diverse forms, including euhedral crystals distributed in petrogenetic minerals such as albite (Figure 8b); lath-like subhedral crystals and disseminated anhedral crystals, which are commonly associated with anhedral zircons (Figures 5c and 8c); crumby anhedral crystals among the albite and aegirine, which are mostly associated with the anhedral zircons and thorite; and, wrapped around albite, K-feldspar, pyrochlore group minerals, and fersmite (Figures 7d and 8d). In the study area, the fergusonite-(Y) is closely related to the pyrochlore group minerals. It was commonly observed that the F-rich pyrochlore is filled with fergusonite-(Y) (Figure 8e,f), and the octahedral F-rich pyrochlore crystals are wrapped by fergusonite-(Y) (Figure 8f).

The fergusonite-(Y) is composed of 19.41–33.58 wt% Y_2O_3, 00.00–4.12 wt% CaO, 0.00–14.37 wt% ThO_2, 47.15–66.42 wt% Nb_2O_5, 0.00–6.93 wt% Ta_2O_5, and 0.00–1.35 wt% TiO_2, with Ta/(Nb + Ta) ratios of 0.006–0.023. The chemical composition of the fergusonite-(Y) in this area is highly variable; is rich in Ca, LREE, Th, and Nb; and is poor in Ta and U.

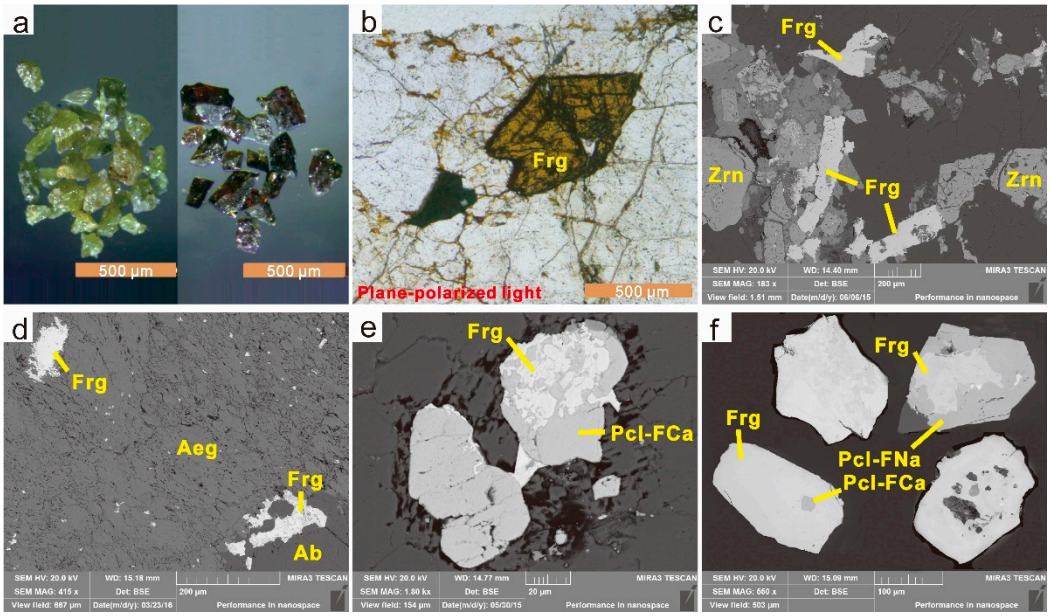

Figure 8. Photomicrographs and BSE images of fergusonite-(Y) with associated minerals. (**a**) Yellowish green and dark brown fergusonite-(Y) crystals; (**b**) photomicrographs of a euhedral fergusonite-(Y) crystal; (**c**) lath-like subhedral fergusonite-(Y) crystals (BSE); (**d**) disseminated anhedral fergusonite-(Y) (BSE); (**e**) disseminated fergusonite-(Y) associated with fluorcalciopyrochlore (BSE); and (**f**) disseminated fergusonite-(Y) associated with fluorcalciopyrochlore and fluornatropyrochlore (BSE). Abbreviations: Ab—albite; Aeg—aegirine; Frg—fergusonite-(Y); Pcl-FCa—fluorcalciopyrochlore; Pcl-FNa—fluornatropyrochlore; Thr—thorite; and Zrn—zircon.

About 100 grains were examined using the EDS method, and more than 215 point-analyses of their chemical compositions were obtained. The compositions are concentrated in the Y and Nb end member of the fergusonite-(Y) zone, as shown in Figure 9.

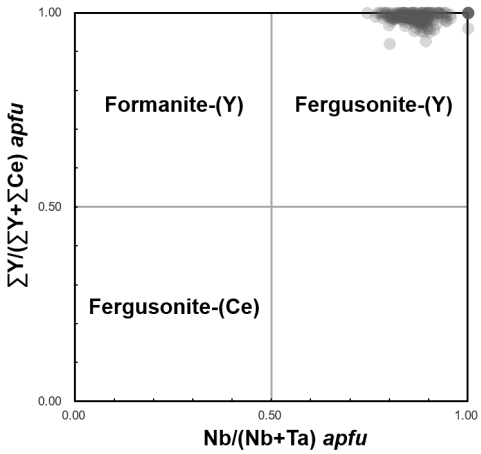

Figure 9. Compositional diagrams (atomic proportion) for the fergusonite-(Y) from the Baicao and Xiaoheiqing deposits.

5.4. Pyrochlore Group Minerals

The pyrochlore group minerals are the main Nb- and Ta-bearing minerals in the syenitic dikes in the study area. The grains are light yellow to dark brown or orange to maroon, primarily occur as euhedral octahedral crystals or allotriomorphic granular particles, and are ~50 to 250 μm in size (Figure 10).

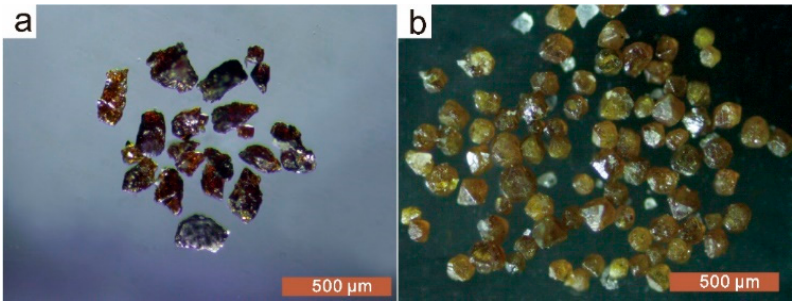

Figure 10. Photomicrographs of pyrochlore group minerals from the Baicao and Xiaoheiqing deposits. (**a**) Allotriomorphic granular particles; and (**b**) euhedral octahedral crystals.

The chemical compositions of the pyrochlore group minerals in our samples are highly variable (Table 1), and the chemical compositions indicate that the pyrochlore group minerals in this area include fluorcalciopyrochlore, fluornatropyrochlore, oxycalciopyrochlore, and "oxynatropyrochlore" (the name not approved by the end of October 2021), according to the classification of the pyrochlore supergroup minerals approved by the Commission on New Minerals, Nomenclature and Classification (CNMNC) of the International Mineralogical Association (IMA) [31].

Table 1. The chemical composition characteristics for the pyrochlore group minerals from the syenitic dikes in the Huili area.

Component (wt%)	Oxycalciopyrochlore	Fluorcalciopyrochlore	"Oxynatropyrochlore"	Fluornatropyrochlore
CaO	12.37–20.17	13.97–20.65	8.85–10.94	11.69–14.9
Na_2O	1.93–6.77	6.24–7.84	5.69–7.59	7.30–8.64
Nb_2O_5	33.50–55.43	43.34–57.69	40.76–49.52	50.22–56.62
Ta_2O_5	1.08–17.62	0.92–13.37	2.46–6.23	2.84–13.72
TiO_2	4.73–12.46	5.68–8.20	6.17–10.41	1.87–7.05
ThO_2	0.25–7.69	0.31–4.46	0.49–3.82	1.12–1.66
UO_2	0.40–16.34	0.04–6.17	3.97–15.55	0.13–3.00
$\sum REE_2O_3$	0.00–11.49	1.17–8.63	9.66–11.33	3.36–11.40
F	1.10–2.28	2.53–3.61	0.86–2.18	2.67–3.19

About 200 grains were examined, and more than 403 chemical composition point analyses were performed. As is shown in Figure 11, the compositions of the pyrochlore group minerals are concentrated in the area near the Nb end member and in the middle of the Na–Ca series, outside of the gap zone proposed by Atencio et al. [31] with 1030 and 840 data points plotted as *A*-sites and *B*-sites, respectively.

The pyrochlore group minerals in this area are not only abundant in quantity and species, but they also exhibit compositional zoning, which is evident in the back-scattered electron images. Four varieties of pyrochlore crystals (pyrochlores I, II, III, and IV), which were formed at different stages, were identified based on their compositional variations, morphologies, zoning, and paragenesis (Figures 12–14). Representative chemical composition data for the pyrochlore group minerals formed at different stages are presented in Table 2. As the *B*-site cations are not considered to be easily leached during weathering and/or hydrothermal activity [60], the pyrochlore compositions are generally expressed with the number of *B*-site cations fixed at 2.0 [31,61–63]. The *apfu* value ranges and averages of the different elements in all the tested pyrochlore group minerals are plotted in Figure 15.

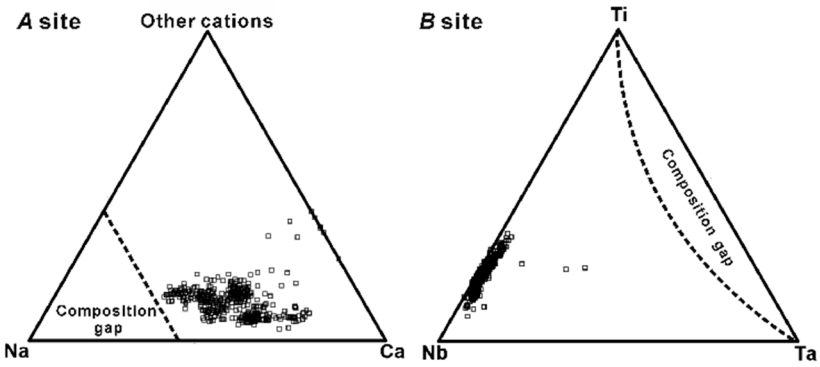

Figure 11. Triangular diagrams of the *A*-site and *B*-site compositions of the pyrochlore group minerals from the Huili area. Other cations denote the other elements and vacancies in the *A*-site. The compositional gap zones represented by the dotted line at the *A*- and *B*-sites were proposed by Atencio et al. [31] using 1030 and 840 analysis data, respectively.

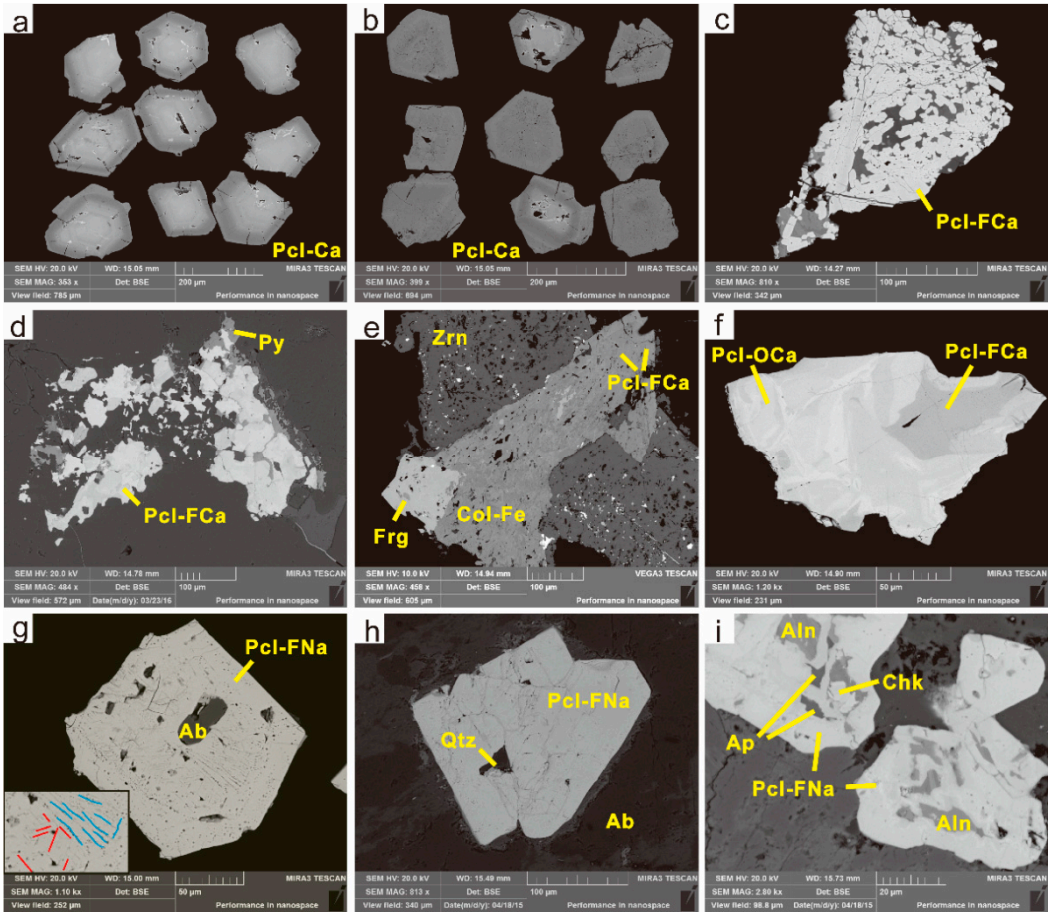

Figure 12. BSE images of the pyrochlore group minerals and associated minerals. (**a**) Calciopyrochlore with fine oscillatory zoning (pyrochlore I); (**b**) calciopyrochlore with oscillatory zoning (pyrochlore II); (**c**) fluorcalciopyrochlore aggregates (pyrochlore II); (**d**) fluorcalciopyrochlore with replacement texture (pyrochlore III); (**e**) an altered columbite-(Fe) crystal replaced by fluorcalciopyrochlore (pyrochlore III); (**f**) fluorcalciopyrochlore with replacement texture (pyrochlore III); (**g**) fluornatropyrochlore with albite and tiny (<1 μm) linear inclusions (pyrochlore IV), the red line represents the straight parting and the blue line represents the curved distribution of holes; (**h**) fluornatropyrochlore with quartz inclusions (pyrochlore IV); and (**i**) REE minerals replaced by fluornatropyrochlore (pyrochlore IV). Abbreviations: Ab—albite; Aln—Allanite-(Ce); Ap—apatite; Chk—chevkinite; Frg—fergusonite-(Y); Col-Fe—columbite-(Fe); Pcl-Ca—calciopyrochlore; Pcl-FCa—fluorcalciopyrochlore; Pcl-OCa—oxycalciopyrochlore; Pcl-FNa—fluornatropyrochlore; Py—pyrite; Qtz—quartz; and Zrn—zircon.

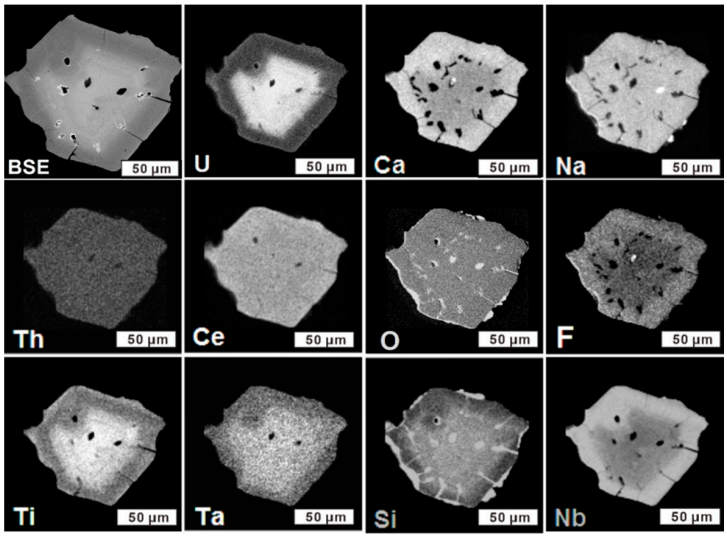

Figure 13. Backscattered electron images and elemental maps of the zoned oxycalciopyrochlore formed in the primary magmatic crystallized stage in the Huili area.

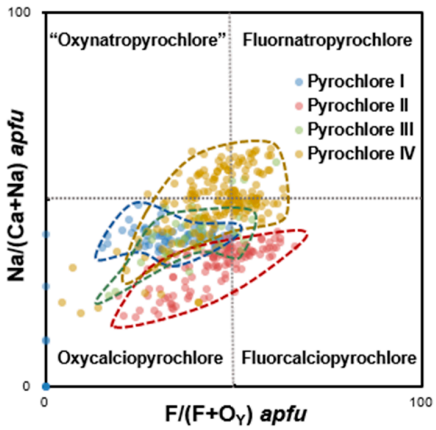

Figure 14. Compositional diagrams (atomic proportion) for the pyrochlore group minerals (pyrochlores I, II, III, and IV) from the Baicao and Xiaoheiqing deposits.

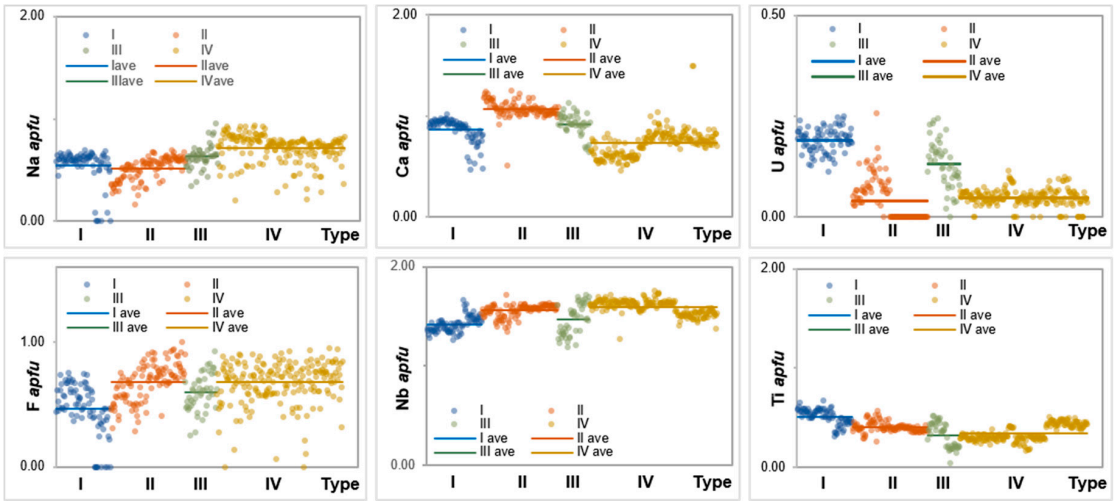

Figure 15. The *apfu* (atoms per formula unit) and its average values of the elements in pyrochlores I, II, III, and IV from the Huili area.

Table 2. Representative electron microprobe data for the pyrochlore group minerals from the syenitic dikes in the Huili area.

Component (wt%)							Formula Coefficients (B = 2)						
Type	**II**	**III**	**IV**	**IV**	**IV**	**IV**	**Type**	**II**	**III**	**IV**	**IV**	**IV**	**IV**
Sample	**XHQ-2**	**BC-23**	**BC-15**	**BC-15**	**BC-13**	**BC-13**	**Sample**	**XHQ-2**	**BC-23**	**BC-15**	**BC-15**	**BC-13**	**BC-13**
Na_2O	2.02	6.99	5.88	6.27	7.51	7.72	Na	0.26	0.87	0.79	0.85	0.98	0.98
CaO	20.30	15.69	12.67	10.73	11.62	14.52	Ca	1.43	1.08	0.94	0.80	0.84	1.01
MgO	0.02	0.00	0.01	0.00	0.01	0.00	Mg	0.00	0.00	0.00	0.00	0.00	0.00
Y_2O_3	1.30	0.37	0.80	1.09	1.78	0.57	Y	0.05	0.01	0.03	0.04	0.06	0.02
ThO_2	8.01	0.83	2.97	3.39	1.17	0.88	Th	0.12	0.01	0.05	0.05	0.02	0.01
Ce_2O_3	3.10	3.57	3.60	5.24	5.46	4.30	Ce	0.07	0.08	0.09	0.13	0.13	0.10
UO_2	0.38	5.64	11.85	5.32	2.89	1.33	U	0.01	0.08	0.18	0.08	0.04	0.02
Pr_2O_3	1.17	0.66	0.71	2.46	1.75	0.66	Pr	0.03	0.02	0.02	0.06	0.04	0.02
PbO	0.00	0.00	0.00	0.04	0.00	0.00	Pb	0.00	0.00	0.00	0.00	0.00	0.00
Nd_2O_3	1.16	1.29	1.44	1.99	1.72	0.92	Nd	0.03	0.03	0.04	0.05	0.04	0.02
La_2O_3	0.28	0.61	0.68	0.87	1.60	0.91	La	0.01	0.01	0.02	0.02	0.04	0.02
SiO_2	0.07	0.03	0.02	0.04	0.00	0.02	$\sum A$-site	2.00	2.20	2.15	2.10	2.20	2.20
							Si	0.00	0.00	0.00	0.00	0.00	0.00
TiO_2	11.88	8.80	10.82	7.98	6.93	4.90	Ti	0.59	0.43	0.56	0.42	0.35	0.24
Nb_2O_5	44.81	51.73	42.78	46.34	51.22	56.95	Nb	1.33	1.51	1.34	1.47	1.56	1.68
Ta_2O_5	1.21	2.73	3.09	2.87	3.04	3.87	Ta	0.02	0.05	0.06	0.05	0.06	0.07
Al_2O_3	0.03	0.03	0.00	0.00	0.01	0.00	Al	0.00	0.00	0.00	0.00	0.00	0.00
MnO	0.78	0.10	0.39	0.50	0.43	0.05	Mn^{2+}	0.04	0.01	0.02	0.03	0.02	0.00
FeO	0.16	0.20	0.35	0.48	0.23	0.18	Fe^{2+}	0.01	0.01	0.02	0.03	0.01	0.01
F	1.37	2.92	1.42	1.93	2.73	3.00	$\sum B$-site	2.00	2.00	2.00	2.00	2.00	2.00
							F in Y-site	0.28	0.59	0.31	0.43	0.58	0.62
$O = F_2$	0.46	1.23	0.60	0.81	1.15	1.26	O in Y-site	0.57	0.40	0.58	0.46	0.41	0.39
Total	97.37	100.96	98.88	96.73	98.95	99.52	Species	OCa	FCa	OCa	ONa	FNa	FCa

5.4.1. Pyrochlores I and II

The pyrochlore I minerals are rich in U, poor in F, and mainly classified oxycalciopyrochlore. The pyrochlore II minerals are poor in U and Na, rich in F, and mainly include oxycalciopyrochlore and fluorcalciopyrochlore. Both pyrochlores I and II minerals formed in the primary magma stage. The element composition of this stage is characterized by an *A*-site that is rich in Ca and poor in Na; a *B*-site that is relatively poor in Nb; and a *Y*-site with a low F content, which mainly includes oxycalciopyrochlore. Pyrochlores I and II are mostly euhedral, generally exhibit concentric zoning (Figure 12a,b) and are mostly distributed in areas less affected by hydrothermal alteration. The concentric zoning is parallel to the crystalline growth face (111) of the crystal and exhibits straight rims. For these types of pyrochlore, the entire grain displays a core-to-shell transitional zoning structure. The outer rim (dark) has comparatively broad zoning, and the core (bright) exhibits weak oscillatory zoning. The dark zoning in the core is comparatively narrow and the bright zoning is comparatively broad. There are a few periods of compositional variation; the element composition is relatively stable, and the chemical composition of the zoning exhibits oscillatory variation characteristics.

The map scanning of the pyrochlore minerals with such zoning indicates that the core (bright) and rim (dark) of the zoning correspond to U-rich and U-poor components, respectively (Figure 13). In the bright zoning of the core, Ta, Si, Ti, and U are synchronously enriched, and the composition was calculated to be oxycalciopyrochlore, i.e., pyrochlore I. In the dark zoning of the rim, F, Ca, and Nb are synchronously enriched and the composition was calculated to be oxycalciopyrochlore or fluorcalciopyrochlore, i.e., pyrochlore II. Na, Th, and Ce are evenly distributed across the grain.

5.4.2. Pyrochlore III

The pyrochlore III minerals are rich in F, Ca, and Na and mainly include Na-rich oxycalciopyrochlore and fluorcalciopyrochlore. The crystals are generally anhedral and replacement textures are commonly observed. Metasomatic relict columbite-(Fe) by pyrochlore III minerals is present but not common (Figure 12d–f).

5.4.3. Pyrochlore IV

The pyrochlore IV minerals are rich in F, Nb, and Na, and vary in species. Natropyrochlore (including fluornatropyrochlore and "oxynatropyrochlore"), F- and Na-rich oxycalciopyrochlore, and Na-rich fluorcalciopyrochlore are uniformly referred to as pyrochlore IV. These minerals are dominant, and they tend to be more concentrated in areas that have undergone strong albitization. The early stage minerals (e.g., apatite, allanite, and chevkinite) were locally or completely replaced by fluids rich in F, Na, and Ca, thus forming pyrochlore IV. Pyrochlore IV minerals are generally anhedral, with occasional metasomatic minerals (Figure 12i). The pyrochlore minerals exhibit irregular flow-component zoning and no contact margins with good self-symmetry occurring among the zoning (Figure 12i). Moreover, Na-rich pyrochlore IV minerals with even compositions were also directly crystallized, with albite, quartz, and tiny (<1 μm) linear inclusions usually observed filled or covered by disseminated or vein-like fergusonite (Figure 8e,f) and surrounded by albite (Figure 12h).

6. Discussion

6.1. The Generation of the Nb–Ta Oxide Minerals

The Nb–Ta-mineralized syenitic dikes in the Panxi region exhibit different stages of Nb–Ta mineral modes. The pyrochlore group minerals formed in the primary magma stage exhibit the characteristics of magmatic fractional crystallization. That is, they are mostly euhedral and generally display oscillatory and transitional zoning structures. Fersmite and columbite-(Fe) crystals are occasionally observed, and fergusonite-(Y) is rare. The pyrochlore group minerals formed in the subsequent fluid-rich stage are generally anhedral

and have replacement textures; large amounts of fergusonite-(Y) occurs; and metasomatic relict columbite-(Fe) and fersmite are present but are not common.

Based on occurrences, the generation of these minerals could be decisively determined. A schematic model of the formation of main Nb–Ta-bearing minerals and Nb–Ta mineralization stages in the Huili syenitic-dike-related Nb–Ta deposits is presented in Figure 16. Fersmite and columbite-(Fe) are the earlier Nb–Ta-bearing minerals, and they typically formed during the magmatic fractional crystallization (Figure 16a,b). Due to the activity of hydrothermal fluids at the late stages of magma evolution, they are characterized by obvious metasomatic residual structures (Figure 16c). The dissolution of these minerals increased the Nb content of the fluid, and pyrite later formed around the dissolved columbite-(Fe) (Figure 5e,f), which may indicate a high f(S) in the hydrothermal stage. The experimental results of Wang et al. [64] revealed that Nb and Ta can be transported as Nb-F and Ta-F complexes, respectively, with Na^+ in aqueous solutions.

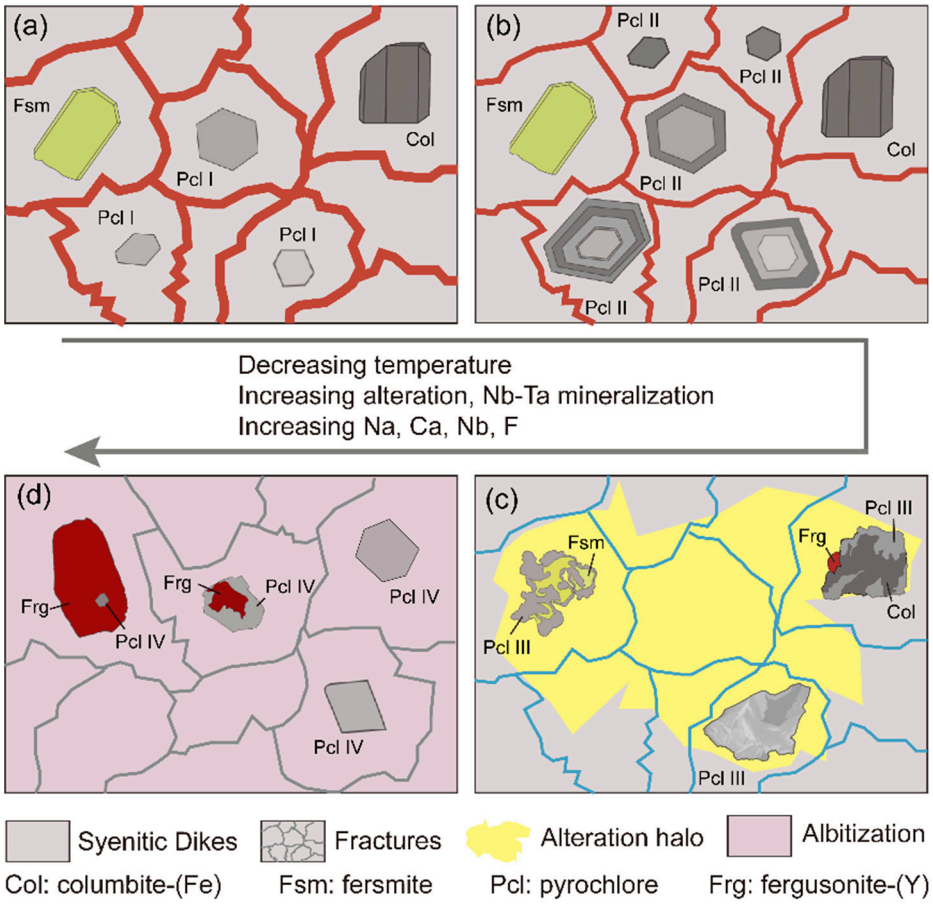

Figure 16. Schematic model of the formation and evolution of Nb–Ta minerals in the Huili Nb–Ta deposits. (**a**) Euhedral pyrochlore I, fersmite, and columbite-(Fe) crystals formed in the primary magma stage; (**b**) the magma gradually accumulated F, Nb, and Ca, resulting in pyrochlore II grew around the pyrochlore I and forming the rim; (**c**) the interaction of the earlier Nb–Ta minerals with magma-derived hydrothermal fluids with high contents of Na, Ca, and F in the late stage of the highly evolved magma; and (**d**) pyrochlore IV crystals associated with fergusonite-(Y) tend to be more concentrated in areas that underwent strong albitization. From (**a**) to (**d**), the Na, Ca, Nb, and F contents of ore-forming fluids increased and the temperatures decreased.

Thus, we suggest that F played a key role in the dissolution. Pyrochlores I and II, which formed in the primary magma stage, mainly include oxycalciopyrochlore. Their *A*-sites are rich in Ca and poor in Na; their *B*-sites are relatively poor in Nb; and their *Y*-sites have low F contents. Figure 13 shows the compositional zoning. The later pyrochlore II is

richer in F and Nb than the earlier pyrochlore I. This positive zoning corresponds well with the evolution of the magmatic-hydrothermal system. That is, as the contents of volatiles such as F increased, the preexisting Nb-bearing minerals (fersmite and columbite-(Fe)) dissolved and the Nb content of the fluid increased.

The pyrochlore III are rich in F, Ca, and Na and mainly include Na-rich oxycalciopyrochlore and fluorcalciopyrochlore. They are generally anhedral with irregular replacement textures around metasomatic relict columbite-(Fe) (Figure 16c), which is consistent with the above hydrothermal transformation. The pyrochlore IV are rich in F, Nb, and Na and tend to be more concentrated in areas that have undergone strong albitization (Figure 16d), which is typical of the auto-metasomatism of the hydrothermal alteration in the Huili syenite dikes [54]. When Na^+ was released from the complexes, the Nb-F and Ta-F complexes decomposed. This was the period of the maximum formation for Nb–Ta mineralization. The fergusonite-(Y) is generally euhedral (Figure 8b) or occurs as veins, exhibiting the characteristics of hydrothermal genesis. It is closely associated with the pyrochlore III and pyrochlore IV minerals. As shown in Figures 5d and 12e, the fergusonite-(Y) occurs with the pyrochlore III and metasomatic relict columbite-(Fe), indicating that it was formed by metasomatism during the fluid-rich stage. Figure 8f shows that the fergusonite-(Y) and pyrochlores IV wrap with each other, indicating that they likely formed in the same period.

In this study, it was found that the pyrochlore supergroup minerals did not only occur in a certain stage of Nb–Ta mineralization but were present from the beginning to the end of the mineralization. Moreover, they formed in the different stages have characteristic chemical compositions and exhibit textural relationships with other minerals. We suggest that the changes in chemical composition and morphologic characteristics for pyrochlore supergroup minerals could serve as a proxy for Nb–Ta mineralization process.

6.2. The Generation of the Pyrochlore Supergroup Minerals

6.2.1. Crystal Chemistry of the Pyrochlore Supergroup Minerals

Compared with the columbite subgroup minerals, which are a better tracer of the evolution of rare metal granites and granite-pegmatites, the pyrochlore supergroup minerals have the same significance for the fluid evolution of alkaline rock type and related carbonatite type Nb–Ta deposits. Due to their unique crystalline structures, the pyrochlore supergroup minerals can accommodate numerous types of cations or additional anions in each site, and thus, by means of ion replacement, they can form a supergroup of numerous mineral species. They have special advantages in terms of studying the variations in the components of the different phases of magma. However, this replacement and combination of ions should still follow the crystal formula laws and the electrovalence equilibrium principles. For example, the pyrochlore minerals in the study area usually contain several ions: Na^+, U^{4+}, Th^{4+}, and Si^{4+}.

In the pyrochlore group minerals, Na usually occurs in the *A*-site in the form of Ca + Na. The statistics of the massive amounts of compositional data show that a compositional gap occurs in the Na end member in the Na–Ca series. The pyrochlore minerals in the Huili area also exhibit this phenomenon, and the Na-dominated *A*-site is mainly distributed in the middle of the Na–Ca series. Atencio et al. [31] attributed the natural clustering of the compositions near Na = Ca = 1 *apfu* to a charge-balancing requirement for members of the B^{5+} groups. Therefore, "oxynatropyrochlore" should not theoretically exist, as its end member ($Na_2Nb_2O_7$) cannot reach electrovalence equilibrium. However, the natropyrochlore in the study area is mainly of hydrothermal metasomatism origin, which led to large amounts of ion impurities in the *A*- and *B*-sites. Thus, according to the new classification scheme for pyrochlore supergroup minerals, the composition in which the *A*-site is dominated by Na, the *B*-site is dominated by Nb, and the *Y*-site is dominated by O, should be classified as "oxynatropyrochlore".

For the existing pyrochlore supergroup minerals, U^{4+}, Th^{4+}, and Si^{4+} are not ion species which can be stable and even dominate in the pyrochlore structure. U^{4+} and Th^{4+} have high charges and large ionic radii, have difficulties in achieving electrovalence

equilibrium, and are usually bringing in additional vacancies, thereby forming crystal defects. With respect to Si^{4+}, some researchers have published data for pyrochlore minerals with a high Si concentration, which supports the idea that Si can be incorporated into the mineral structure as a result of replacement reactions [65,66]. Moreover, Bonazzi et al. [67] indicated that 30–50% of the Si occupies the octahedral sites of the pyrochlore structure, but a larger fraction (50–70%) of Si is distributed in the radiation-damaged portions of the sample. Therefore, U, Th, and Si are not favorable for the stabilization of the crystal structure, whereas Nb, Ta, and Ca+Nb are easier to get into to the pyrochlore lattice, which is consistent with the actual mineral occurrence. Thus, the increased concentrations of Na, U, Th, and Si in the structure of the pyrochlore group minerals can directly reflect the enrichment of Na, U, Th, and Si in the fluids and can also indirectly reflect the variations in the Ca and Nb concentrations of the fluids.

6.2.2. Pyrochlore Group Minerals Evolution vs. the Magmatic-Hydrothermal Evolution of the Syenitic Dikes

Based on a comparison of the variations in the *apfu* values of the main components (Table 2 and Figure 15), the chemical compositions of pyrochlores I to IV exhibit the following characteristics.

A-site cations: the Na content is stable in pyrochlore I and gradually increases from pyrochlores II to IV. The Ca content is comparatively low in pyrochlore I, reaches its peak in pyrochlore II, and gradually decreases from pyrochlores III to IV. The U content is highest in the pyrochlore I minerals. *B*-site cations: the Nb content is lowest in pyrochlore I and highest in pyrochlore IV. The average Ti content is largest in pyrochlore I, and the Ti contents are stable and similar from pyrochlores II to IV. However, the Nb and Ti contents of pyrochlore III vary over a broad range. *Y*-site ions: the F content of pyrochlore I is the lowest on average, and the F contents of some samples of pyrochlores II to IV are close to a full occupation of the *Y*-site.

According to the variation in the *apfu* values of the different ions in the pyrochlore group minerals crystallized in the four different phases, as well as the map scanning distribution of the elements, it is speculated that pyrochlore I crystalized from melts with Ti, U, Ta, and Si contents that were comparatively higher than those of the later-stage, while the F, Ca, Na, and Nb contents were comparatively lower. During this phase (Phase I), U^{4+}, Ti^{4+}+Si^{4+}, and O^{2-} partly occupied the *A*-, *B*-, and *Y*-sites in pyrochlore I, respectively. After massive amounts of minerals were crystallized, the melts gradually accumulated F, Nb, and Ca, resulting in secondary growth around the pyrochlore I and forming the aforementioned rim, which is comparatively rich in F, Nb, and Ca. This rim is composed of pyrochlore II (Figure 12a,b). In addition, pyrochlore II with a homogeneous composition was also directly crystallized out of the magma (Figure 12b,c). In pyrochlore II, Ca, Nb, and F predominantly occupied the *A*-, *B*-, and *Y*-sites and replaced the ionic impurities via substitution vector $U^{4+} + Ti^{4+} + O^{2-} \rightarrow Ca^{2+} + Nb^{5+} + F^{-}$. In this phase, the Na content of the pyrochlore structure did not increase in the way of Na in melts, as the Na in the crystal lattices of the pyrochlore group minerals was not a superior occupying ion as was previously described.

In Phase III, with melts exsolving large amounts of fluids, F, Na, and Ca became further enriched in the magma-derived hydrothermal fluids. During the early stage of the metasomatism, the Ca replaced the early stage minerals, which is supported by the fact that the associated thorite was also replaced by Ca-rich fluids, likely associated with the substitution vector $Th^{4+} + O^{2-} \rightarrow Ca^{2+} + H_2O$. In this stage, due to the intense metasomatism, the chemical compositions of the minerals varied greatly. F continued to enter the crystal lattices of the pyrochlore minerals by means of a $Ca^{2+} + O^{2-} \rightarrow Na^{+} + F^{-}$ substitution, which also brought more Na into the crystal lattice, leading to decreased Ca in the crystal lattices. In addition, pyrochlore III were mainly of metasomatic origin with the major precursor being Nb–Ta oxides such as columbite-(Fe). Thus, Pyrochlore III vary greatly in composition.

Pyrochlore IV crystallized in the albitization stage (Phase IV), during which Na and F gradually dominated the *A*- and *Y*-sites of the pyrochlore structures through the Ca^{2+} + $O^{2-} \rightarrow Na^{+} + F^{-}$ substitution. Pyrochlore IV mostly have a self-crystallization origin and have high F and Na contents, resulting in the main products being fluornatropyrochlore and Na-F-rich calciopyrochlore. The others are of replacement origin, and the metasomatic minerals include apatite, allanite and chevkinite, leading to high contents of Si, Ti, and P in the *B*-site. Moreover, this type of pyrochlore IV has significantly variable Ca and Na contents in the *A*-site and O and F contents in the *Y*-site.

Above all, throughout the entire magma evolution process, the main element replacement mechanisms involved in the formation and alteration of the pyrochlore group minerals in the study area were as follows:

$$U^{4+} + Ti^{4+} + O^{2-} \rightarrow Ca^{2+} + Nb^{5+} + F^{-},$$

$$Ca^{2+} + O^{2-} \rightarrow Na^{+} + F^{-}.$$

In the Nb–Ta mineralized syenitic dikes in the Huili area, the pyrochlore group minerals that crystallized in the different phases exhibited a gradual enrichment in fluorine. To verify the aforementioned speculation, the correlations between the different ions in pyrochlores I to IV were analyzed (Figure 17).

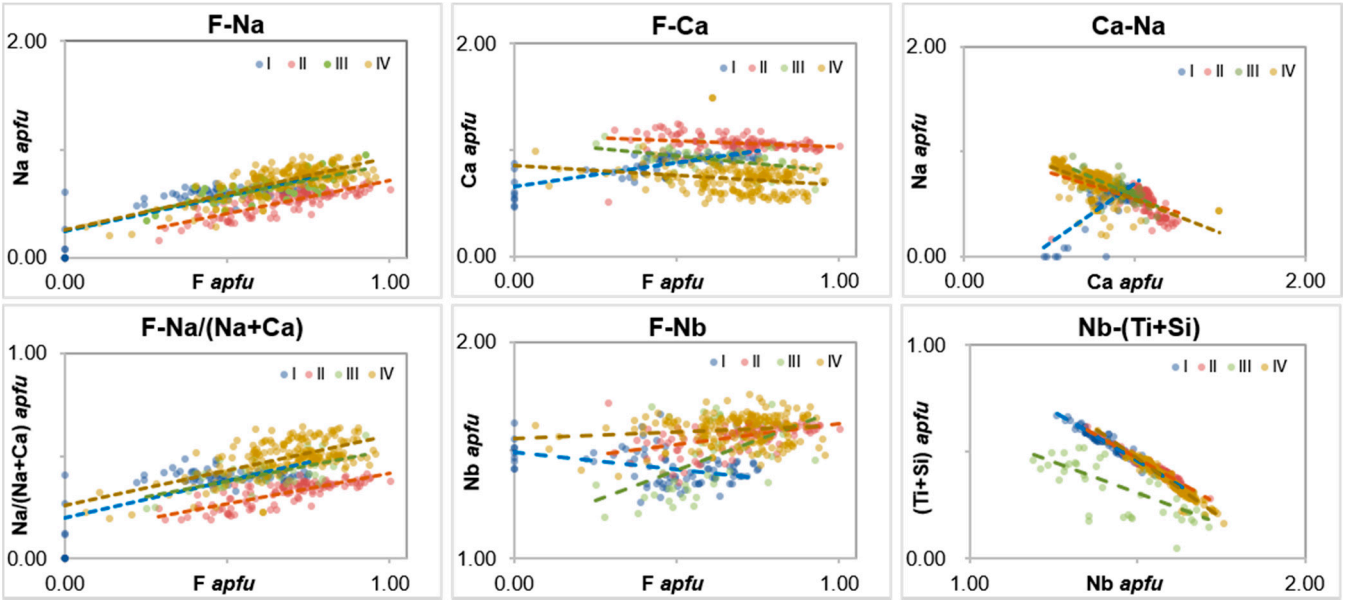

Figure 17. Binary plots illustrating the compositions (*apfu*) of the pyrochlore group minerals from the Huili area.

In the four phases, F and Na exhibit a strong positive correlation with a consistent slope, and pyrochlore II generally have low Na contents. The F and Ca contents exhibit a positive correlation in pyrochlore I, while they exhibit slope-consistent negative correlations in pyrochlores II to IV. Thus, this indicates that in the late stage of magma evolution, the F, Na, and Ca underwent a gradual enrichment process. The F, Na, and Ca contents of the early magma were low, and ion groups such as F + Na + Ca and Ti + U + Ta + Si competed to enter the crystal lattices of the pyrochlore group minerals. As the magma evolution progressed, the F and Na contents gradually increased and Na and Ca started to compete. However, when F + Na + Nb participated in the crystallization simultaneously, the existence of Ca was necessary to achieve electrovalence equilibrium in the crystal lattices, i.e., $(Ca_{2-x},Na_x)_{\sum 2}Nb_2O_6(O_{1-x},F_x)_{\sum 1}$, $(0 \leq x \leq 1)$.

Except for the negative correlation in pyrochlore I, the correlations between F and Nb were positive in pyrochlores II to IV, but the slope was much larger for pyrochlore III. Based on the abnormal contents of several of the ions in pyrochlore III (Figure 15), it is speculated

that during the early metasomatism, the minerals in the surrounding syenite intrusions underwent metasomatic reactions with the fluids; the varying degrees of the reaction resulted in the significant variations in the F, Ca, Na, Nb, and Ti contents of pyrochlore III.

6.3. Two Stages of Crystallization of Nb–Ta Minerals in the Huili Syenite Dikes

Massive pegmatitic ore-bearing syenite dikes occur in the Huili area, indicating that the magma system entered the magmatic-hydrothermal transition stage [68]. According to textural and compositional characteristics, Nb–Ta oxide minerals in the Huili syenite dikes could be further divided into two stages: the primary magmatic mineralization stage and the fluid-rich mineralization stage.

6.3.1. Primary Magmatic Mineralization Stage

The occurrence of abundant pyrochlore group minerals (ore minerals) indicates that the ore-rich dikes were enriched in volatiles such as H_2O and F during their formation. Several studies [69,70] have noted that in the magma stage, pyrochlore stably crystallizes earlier than other Nb-bearing minerals, when the fluorine exists in the magma system. Thus, the occurrence of early columbite-(Fe) and fersmite in the syenite dikes in the Huili area suggests that during the magmatic-hydrothermal evolution process, the magma originally lacked volatiles, and as the magma highly evolved, it was relatively enriched in F-dominated volatiles, giving rise to pyrochlore-type Nb–Ta minerals. In addition, the pyrochlore particles in the Nb–Ta-mineralized syenitic dikes contain 0.86–3.61 wt% F, indicating that the magma of the Nb–Ta-mineralized syenitic dikes may have been rich in fluids/volatiles, which also supports that the Nb–Ta mineralized syenitic dikes formed from the highly evolved magma. The variation in the F content reflects the magma evolution process of the whole magmatic-hydrothermal transition stage [23,58,71], and it played a key role in the enrichment and mineralization of Nb and Ta ions. Moreover, it is concluded that the enrichment of F in the fluids also played an important role in controlling the variable components of the pyrochlore group minerals.

The euhedral pyrochlore I and II crystals with oscillatory and transitional zoning structures mainly formed during the primary magmatic mineralization stage (Figure 16a,b). The crystal shapes are comparatively regular, and the straight zoned rims are nearly parallel to the crystal faces. The compositions of the transitional zoning structure are consistent without abrupt changes in ion species. This zoning can only be developed in self-crystallized pyrochlore group minerals in a comparatively stable environment. Therefore, this should be the result of equilibrium fractional crystallization during normal geochemical evolution [51]. Barsanov et al. [72] concluded that this oscillatory zoning structure was formed by the incomplete miscibility of two end-member components of the Nb–Ta series (Nb and Ta). Norton and Dutrow [73] studied the complicated behaviors of magmatic-hydrothermal processes and concluded that magmatic-hydrothermal processes involve a complex dynamic system, in which the existence of a supercritical fluid may transform the system into a disordered state, but this system provides the dynamic conditions required to form an oscillatory zoning structure. We believe that the oscillatory zoning structures of the pyrochlore group minerals reflect a complicated crystallization history and conditions, and they were formed through disequilibrium crystallization in an oscillatory environment.

6.3.2. Fluid-Rich Mineralization Stage

In the late stage of the highly evolved magma, melts exsolve large amounts of fluids (Figure 16c,d). The magma-derived hydrothermal fluids were enriched in fluorine, giving rise to pyrochlore-type Nb–Ta minerals. Besides, the irregular patterns of zoning are also linked to the interaction of the earlier Nb–Ta minerals with magma-derived hydrothermal fluids at the late stages of magma evolution.

The phenomena that the rim of the transitional zoning has a higher Nb and F than the core (Figure 13), and that the pyrochlore crystals in the fluid-rich stage (pyrochlores III and IV) have Nb and F contents higher than those in the primary magma stage (pyrochlores

I and II) (Table 2 and Figure 15), both indicate that Nb and F were gradually enriched in the late stage of the highly evolved magma, probably due to the incompatibility of Nb_2O_5 in the melt. Moreover, the pyrochlore crystals that crystallized during the fluid-rich stage (pyrochlores III and IV) have higher Na_2O and lower CaO contents than those that crystallized in the primary magma stage (pyrochlores I and II) (Table 2 and Figure 15). In pyrochlores I to IV, fluorine is positively correlated with Nb and Na (Figure 17), indicating that the enrichment of Nb in the highly evolved magma was likely related to the increases in Na and F.

Nb and Ta are generally poorly soluble in aqueous solutions [74]. However, the solubility and hydrothermal transfer of Ta and Nb are greatly enhanced in F-rich solutions under reducing conditions [74]. Experiments with Na^+ in aqueous solutions have shown that Nb and Ta can be transported as Nb-F and Ta-F complexes [62,64,75]. The presence of Na can increase Nb's solubility, but Na alone is not sufficient. In the absence of H_2O and F in the system, Nb is poorly soluble. F plays an important role in effectively improving the solubility of Nb and Ta and reducing the liquidus temperature [70,76,77]. However, the solubility of NaF is limited in high-temperature water-bearing fluids, and the precipitation of minerals containing fluorine or the reduction in the fluorine concentration due to the influence of other fluids can lead to albitization in rocks [16] (Figure 16d). When F^- is released from the complexes, the Nb-F and Ta-F complexes decompose, causing the Nb and Ta to crystallize into minerals.

6.4. Types of Minerals in the Different Types of Felsic Nb–Ta Deposits

The types of Nb–Ta minerals in granite- and pegmatite-type and syenite-type Nb–Ta deposits have their own characteristics. In highly evolved granites and pegmatites, columbite ($(Fe,Mn)Nb_2O_6$) and tantalite ($(Fe,Mn)Ta_2O_6$) group minerals are the main Nb- and Ta-bearing minerals [10,17,78–83], i.e., in the form of Nb–Ta oxides composed of transition metal elements. For syenite type deposits, pyrochlore supergroup minerals and fergusonite group minerals are the main ore-hosting minerals, i.e., the Nb–Ta oxides composed of alkali metal elements (e.g., Ca, Na) or REEs (e.g., Y) [15,84,85].

A comparison of alkaline rock type (including alkaline granite type and alkaline pegmatite type) Nb–Ta deposits with other rare element granite type and pegmatite type Nb–Ta deposits emphasizes the importance of albitization. Granite type and pegmatite type Nb–Ta deposits exhibit stronger crystalline fractionation signatures [23,25,27,51,71], but alkaline rock type deposits (especially syenite type Nb–Ta deposits) are of variable genesis and are the result of fractional crystallization and more significant hydrothermal metasomatism, especially albitization. This albitization is closely related to the mineralization and is an inevitable product of the late melt-fluid stage of the magma evolution based on Nb–Ta enrichment through magmatic fractional crystallization.

Above all, the contributions of hydrothermal metasomatism (especially albitization) to Nb–Ta enrichment of syenitic dike type deposits are concluded to be as follows: (1) the enrichment of Nb and Ta, acting as carriers and extracting the Nb and Ta from the early stage Nb–Ta minerals; (2) destroying the Nb–Ta-bearing complexes, thus causing Nb–Ta minerals to crystallize and separate out; and (3) gradually transforming the occurrence mode of the Nb and Ta and the species of Nb–Ta minerals.

7. Conclusions

(1) The evolution of Nb–Ta oxide minerals within a syenitic-dike-related magmatic-hydrothermal system was studied on the examples of the Baicao and Xiaoheiqing deposits, in the Huili area. The mineralogical phenomena observed in the Huili syenite dikes provide strong evidence that the magmatic-hydrothermal transitional stage, including the primary magmatic mineralization stage and the fluid-rich mineralization stage, is a favored model for explaining the Nb–Ta mineralization process.

(2) Pyrochlore supergroup minerals can record melt evolution and hydrothermal alteration through changes in chemical compositions, texture characteristics, crystal structures,

and geochemical and petrographic characteristics. As the main Nb–Ta-bearing minerals for syenitic-dike-related Nb–Ta deposits, the pyrochlore supergroup minerals have unique crystal chemistry characteristics and form throughout the entire Nb–Ta mineralization process, which are of great significance to understanding the Nb–Ta mineralization process.

Author Contributions: Conceptualization, Y.X. and G.L.; methodology, Y.X.; validation, G.L., Y.X. and N.S.; investigation, Y.X.; data curation, Y.X. and N.S.; writing—original draft preparation, Y.X. and N.S.; writing—review and editing, G.L.; visualization, Y.X. and N.S.; supervision, G.L.; funding acquisition, G.L. and Y.X. All authors have read and agreed to the published version of the manuscript.

Funding: This research has been supported by the National Natural Science Foundation of China (grant no. 41672043) and the China National Postdoctoral Program for Innovative Talents (grant no. BX20190304).

Acknowledgments: We thank Ge Xiangkun (Beijing Research Institute of Uranium Geology) for the chemical analysis. We acknowledge Qiu Kunfeng (China University of Geosciences (Beijing)) for his valuable suggestions for this manuscript.

Conflicts of Interest: The authors declare no conflict of interest.

References

1. Ballouard, C.; Massuyeau, M.; Elburg, M.A.; Tappe, S.; Viljoen, F.; Brandenburg, J.T. The magmatic and magmatic-hydrothermal evolution of felsic igneous rocks as seen through Nb-Ta geochemical fractionation, with implications for the origins of rare-metal mineralizations. *Earth-Sci. Rev.* **2020**, *203*, 103115. [CrossRef]
2. Linnen, R.L.; Samson, I.M.; Williams-Jones, A.E.; Chakhmouradian, A.R. Geochemistry of the rare-earth element, Nb, Ta, Hf, and Zr deposits. In *Treatise on Geochemistry*, 2nd ed.; Scott, S.D., Ed.; Elsevier Science: Amsterdam, The Netherlands, 2014; pp. 543–568.
3. Linnen, R.L.; Trueman, D.L.; Burt, R. *Critical Metals Handbook*; Gunn, G., Ed.; John Wiley & Sons: Hoboken, NJ, USA, 2014; pp. 361–384.
4. Bonin, B. A-type granites and related rocks: Evolution of a concept, problems and prospects. *Lithos* **2007**, *97*, 1–29. [CrossRef]
5. Collins, W.J.; Beams, S.D.; White, A.J.R.; Chappell, B.W. Nature and origin of A-type granites with particular reference to southeastern Australia. *Contrib. Mineral. Petrol.* **1982**, *80*, 189–200. [CrossRef]
6. Whalen, J.B.; Currie, K.L.; Chappell, B.W. A-type granites: Geochemical characteristics, discrimination and petrogenesis. *Contrib. Mineral. Petrol.* **1987**, *95*, 407–419. [CrossRef]
7. Černý, P.; Ercit, T.S. The classification of granitic pegmatites revisited. *Can. Mineral.* **2005**, *43*, 2005–2026. [CrossRef]
8. Chakhmouradian, A.R.; Zaitsev, A.N. Rare earth mineralization in igneous rocks: Sources and processes. *Elements* **2012**, *8*, 347–353. [CrossRef]
9. Linnen, R.L.; Cuney, M. Granite-related rare-element deposits and experimental constraints on Ta-Nb-W-Sn-Zr-Hf mineralization, in Linnen RL and Samson IM, eds., rare-element geochemistry and mineral deposits. *Geol. Assoc. Can. GAC Short Course* **2005**, *17*, 45–67.
10. Linnen, R.L.; Keppler, H. Columbite solubility in granitic melts: Consequences for the enrichment and fractionation of Nb and Ta in the Earth's crust. *Contrib. Mineral. Petrol.* **1997**, *128*, 213–227. [CrossRef]
11. Linnen, R.L. The solubility of Nb-Ta-Zr-Hf-W in granitic melts with Li and Li + F; constraints for mineralization in rare metal granites and pegmatites. *Econ. Geol.* **1998**, *93*, 1013–1025. [CrossRef]
12. Zhu, Z.Y.; Wang, R.C.; Marignac, C.; Cuney, M.; Lespinasse, M. Petrogenesis of Nb–(Ta) aplo-pegmatites and fine-grained granites from the Early Cretaceous Huangshan rare-metal granite suite, northeast Jiangxi Province, southeast China. *Lithos* **2019**, *346–347*, 105150. [CrossRef]
13. Cuney, M.; Marignac, C.; Weisbrod, A. The Beauvoir topaz-lepidolite albite granite (Massif Central, France); the disseminated magmatic Sn-Li-Ta-Nb-Be mineralization. *Econ. Geol.* **1992**, *87*, 1766–1794. [CrossRef]
14. Hildreth, W. The Bishop Tuff: Evidence for the origin of compositional zonation in silicic magma chambers. *Geol. Soc. Am. Spec. Pap.* **1979**, *180*, 43–75.
15. Kovalenko, V.I.; Tasryeva, G.M.; Goreglyad, A.V.; Yarmolyuk, V.V.; Troitsky, V.A. The peralkaline granite-related Khaldzan-Buregtey rare metal (Zr, Nb, REE) deposit, western Mongolia. *Econ. Geol.* **1995**, *90*, 530–547. [CrossRef]
16. Pollard, P.J. Geochemistry of granites associated with tantalum and niobium mineralization. In *Lanthanides, Tantalum and Niobium*; Möller, P.Č.P., Saupé, F., Eds.; Springer: Berlin/Heidelberg, Germany, 1989; pp. 145–168.
17. Raimbault, L.; Cuney, M.; Azencott, C.; Duthou, J.L.; Joron, J.L. Geochemical evidence for a multistage magmatic genesis of Ta-Sn-Li mineralization in the granite at Beauvoir, French Massif Central. *Econ. Geol.* **1995**, *90*, 548–576. [CrossRef]
18. Zhu, J.C.; Li, R.K.; Li, F.C.; Xiong, X.L.; Zhou, F.Y.; Huang, X.L. Topaz–albite granites and rare-metal mineralization in the Limu district, Guangxi Province, southeast China. *Miner. Depos.* **2001**, *36*, 393–405. [CrossRef]

19. Kempe, U.; Gotze, J.; Dandar, S.; Habermann, D. Magmatic and metasomatic processes during formation of the Nb-Zr-REE deposits Khaldzan Buregte and Tsakhir (Mongolian Altai): Indications from a combined CL-SEM study. *Mineral. Mag.* **1999**, *63*, 165–177. [CrossRef]
20. Salvi, S.; Williams-Jones, A.E. Alteration, HFSE mineralisation and hydrocarbon formation in peralkaline igneous systems: Insights from the Strange Lake Pluton, Canada. *Lithos* **2006**, *91*, 19–34. [CrossRef]
21. Alexander, P.G.; Anthony, E.W.; Patrick, C. Lithogeochemical vectors for hydrothermal processes in the strange lake peralkaline granitic REE-Zr-Nb deposit. *Econ. Geol.* **2016**, *111*, 1241–1276.
22. Beurlen, H.; Da Silva, M.R.R.; Thomas, R.; Soares, D.; Olivier, P. Nb–Ta–(Ti–Sn) oxide mineral chemistry as tracer of rare-element granitic pegmatite fractionation in the Borborema Province, Northeastern Brazil. *Miner. Depos.* **2008**, *43*, 207–228. [CrossRef]
23. Breiter, K.; Korbelová, Z.; Chládek, Š.; Uher, P.; Knésl, I.; Rambousek, P.; Hönig, S.; Sesulka, V. Diversity of Ti–Sn–W–Nb–Ta oxide minerals in the classic granite-related magmatic–hydrothermal Cínovec/Zinnwald Sn–W–Li deposit (Czech Republic). *Eur. J. Mineral.* **2017**, *29*, 727–738. [CrossRef]
24. Khromova, E.A.; Doroshkevich, A.G.; Sharygin, V.V.; Izbrodin, L.A. Compositional evolution of pyrochlore-group minerals in carbonatites of the Belaya Zima Pluton, Eastern Sayan. *Geol. Ore Depos.* **2017**, *59*, 752–764. [CrossRef]
25. Rao, C.; Wang, R.C.; Hu, H.; Zhang, W.L. Complex internal textures in oxide minerals from the Nanping No. 31 dyke of granitic pegmatite, Fujian Province, southeastern China. *Can. Mineral.* **2009**, *47*, 1195–1212. [CrossRef]
26. Van Lichtervelde, M.; Salvi, S.; Béziat, D.; Linnen, R. Textural features and chemical evolution in tantalum oxides: Magmatic versus hydrothermal origins for Ta mineralization in the Tanco Lower Pegmatite, Manitoba, Canada. *Econ. Geol.* **2007**, *102*, 257–276. [CrossRef]
27. Zhu, Z.Y.; Wang, R.C.; Che, X.D.; Zhu, J.C.; Wei, X.L.; Huang, X.E. Magmatic–hydrothermal rare-element mineralization in the Songshugang granite (northeastern Jiangxi, China): Insights from an electron-microprobe study of Nb–Ta–Zr minerals. *Ore Geol. Rev.* **2015**, *65*, 749–760. [CrossRef]
28. Anenburg, M.; Mavrogenes, J.A.; Frigo, C.; Wall, F. An experimental approach to examine fluid-melt interaction and mineralization in rare-metal pegmatites. *Sci. Adv.* **2020**, *6*, eabb6570. [CrossRef]
29. Sami, M.; Mahdy, N.M.; Ntaflos, T.; Fathy, D. Composition and origin of Ti–Nb–Ta–Zr bearing minerals in the abu diab highly evolved granite from the Central Eastern Desert of Egypt. *J. Afr. Earth Sci.* **2020**, *165*, 103808. [CrossRef]
30. Carl, S.; Caitlin, M. Geology and genesis of the Toongi rare metal (Zr, Hf, Nb, Ta, Y and REE) deposit, NSW, Australia, and implications for rare metal mineralization in peralkaline igneous rocks. *Contrib. Mineral. Petrol.* **2016**, *171*, 104.
31. Atencio, D.; Andrade, M.B.; Christy, A.G.; Giere, R.; Kartashov, P.M. The pyrochlore supergroup of minerals: Nomenclature. *Can. Mineral.* **2010**, *48*, 673–698. [CrossRef]
32. Jamie, A.M.; Adrian, A.F.; Donald, A.H.; Ashlyn, A.B. Geochemistry of pyrochlore minerals from the Motzfeldt Center, South Greenland: The mineralogy of a syenite-hosted Ta, Nb deposit. *Am. Mineral.* **2013**, *98*, 426–438.
33. Walter, B.F.; Parsapoor, A.; Braunger, S.; Marks, M.A. Pyrochlore as a monitor for magmatic and hydrothermal processes in carbonatites from the Kaiserstuhl volcanic complex (SW Germany). *Chem. Geol.* **2018**, *498*, 1–16. [CrossRef]
34. Yan, D.P.; Zhou, M.F.; Song, H.L.; Wang, X.W.; Malpas, J. Origin and tectonic significance of a Mesozoic multi-layer over-thrust system within the Yangtze Block (South China). *Tectonophysics* **2003**, *361*, 239–254. [CrossRef]
35. Wang, C.Y.; Zhou, M.F.; Zhao, D.G. Fe–Ti–Cr oxides from the Permian Xinjie mafic–ultramafic layered intrusion in the Emeishan large igneous province, SW China: Crystallization from Fe-and Ti-rich basaltic magmas. *Lithos* **2008**, *102*, 198–217. [CrossRef]
36. Shellnutt, J.G.; Iizuka, Y. Oxidation zonation within the Emeishan large igneous province: Evidence from mantle-derived syenitic plutons. *J. Asian Earth Sci.* **2012**, *54*, 31–40. [CrossRef]
37. Chung, S.L.; Jahn, B.M. Plume-lithosphere interaction in generation of the Emeishan flood basalts at the Permian-Triassic boundary. *Geol. Fujian* **1995**, *23*, 889–892. [CrossRef]
38. He, J.L. Ore-forming Geological Conditions and Prospecting Potential for Nb-Ta Mineral Deposits in Panzhihua-Xichang Region, Sichuan. *Acta Geol. Sichuan* **2004**, *4*, 206–211.
39. Pang, K.N.; Li, C.; Zhou, M.F.; Ripley, E.M. Mineral compositional constraints on petrogenesis and oxide ore genesis of the late Permian Panzhihua layered gabbroic intrusion, SW China. *Lithos* **2009**, *110*, 199–214. [CrossRef]
40. Xing, C.M.; Wang, C.Y.; Zhang, M.J. Volatile and CHO isotopic compositions of giant Fe-Ti-V oxide deposits in the Panxi region and their implications for the sources of volatiles and the origin of Fe-Ti oxide ores. *Sci. China Earth Sci.* **2012**, *55*, 1782–1795. [CrossRef]
41. Zhong, H.; Zhu, W.G.; Chu, Z.Y.; He, D.F.; Song, X.Y. SHRIMP U–Pb zircon geochronology, geochemistry, and Nd–Sr isotopic study of contrasting granites in the Emeishan large igneous province, SW China. *Chem. Geol.* **2007**, *236*, 112–133. [CrossRef]
42. Xu, Y.G.; Luo, Z.Y.; Huang, X.L.; He, B.; Xiao, L.; Xie, L.W.; Shi, Y.R. Zircon U–Pb and Hf isotope constraints on crustal melting associated with the Emeishan mantle plume. *Geochim. Cosmochim. Acta* **2008**, *72*, 3084–3104. [CrossRef]
43. Coffifin, M.F.; Eldholm, O. Large igneous provinces: Crustal structure, dimensions, and external consequences. *Rev. Geophys.* **1994**, *32*, 1–36. [CrossRef]
44. Jerram, D.A.; Widdowson, M. The anatomy of Continental Flood Basalt Provinces: Geological constraints on the processes and products of flood volcanism. *Lithos* **2005**, *79*, 385–405. [CrossRef]

45. Shellnutt, J.G.; Wang, C.Y.; Zhou, M.F.; Yang, Y.H. Zircon Lu–Hf isotopic compositions of metaluminous and peralkaline A-type granitic plutons of the Emeishan large igneous province (SW China): Constraints on the mantle source. *J. Asian Earth Sci.* **2009**, *35*, 45–55. [CrossRef]
46. Xu, Y.G.; Chung, S.L.; Jahn, B.M.; Wu, G.Y. Petrologic and geochemical constraints on the petrogenesis of Permian–Triassic Emeishan flood basalts in southwestern China. *Lithos* **2001**, *58*, 145–168. [CrossRef]
47. Zhou, M.F.; Yan, D.P.; Kennedy, A.K.; Li, Y.Q.; Ding, J. SHRIMP U–Pb zircon geochronological and geochemical evidence for Neoproterozoic arc-magmatism along the western margin of the Yangtze Block, South China. *Earth Planet. Sci. Lett.* **2002**, *196*, 51–67. [CrossRef]
48. Xiao, L.; Pirajno, F.; He, Q. A preliminary discussion on large igneous provinces and associated ore deposits. *Geol. J. China Univ.* **2007**, *13*, 148.
49. Li, W.Y.; Niu, Y.L.; Zhang, Z.W.; Zhang, M.J.; Gao, Y.B.; Hu, P.Q.; Zhang, J.W.; Tan, W.T.; Jiang, H.B. Geodynamic setting and further exploration of magmatism related mineralization concentrated in the Late Paleozoic in the northern Xinjiang Autonomous Region. *Earth Sci. Front.* **2012**, *19*, 41.
50. Wang, F.L.; Zhao, T.P.; Chen, W. Advances in study of Nb-Ta ore deposits in Panxi area and tentative discussion on genesis of these ore deposits. *Miner. Depos.* **2012**, *31*, 293–308.
51. Zhang, A.C.; Wang, R.C.; Hu, H.; Zhang, H.; Zhu, J.C.; Xie, L. The complex zonation of columbite-group minerals from the Koktokay No. 3 granitic pegmatite dyke, Altay, NW China and its petrological implications. *Acta Geol. Sin.* **2004**, *2*, 181–189.
52. Wang, F.L.; Zhao, T.P.; Chen, T.W.; Wang, Y. Zircon U–Pb ages and Lu–Hf isotopic compositions of the Nb–Ta–Zr-bearing syenitic dikes in the Emeishan large igneous province. *Acta Petrol. Sin.* **2013**, *29*, 3519–3532.
53. Yang, Z.S.; Duan, H.M.; Wang, X.J. Geological features and range of reconnaissance of Nb-Ta deposits in the Panzhihua-Xichang Region, Sichuan. *Acta Geol. Sichuan* **2007**, *27*, 248–254.
54. Wang, F.L.; Zhao, T.P.; Wang, Y. Petrogenisis of Permian Nb–Ta mineralized syenitic dikes in the Panxi district, SW China. *Acta Petrol. Sin.* **2015**, *31*, 1797–1805.
55. Xichang Geological Team in the Sichuan Bureau of Geology. *The Lecture of Detail Exploration about Baicao Nb, Ta Deposit in the Panxi Region*; Unpublished work; 1962.
56. Liu, J.D.; Zhang, C.J.; Li, Y.G.; Liu, X.F.; Yang, Z.X.; Ma, X.Y.; Kan, Z.Z.; Chen, C.D. *Metallization Systems in the Panzhihua-Xichang area of Sichuan, China*; Geological Publishing House: Beijing, China, 2007.
57. Wei, B.; Wang, C.Y.; Zhao, Z.; Bao, H. Columbite-group minerals and mica of peraluminous granite record the magmatic-hydrothermal processes that formed the Zhaojinggou TaNb deposit in the North China Craton. *Lithos* **2020**, *370*, 105648. [CrossRef]
58. Wu, H.; Huang, H.; Zhang, Z.; Wang, T.; Wang, W. Geochronology, geochemistry, mineralogy and metallogenic implications of the Zhaojinggou Nb-Ta deposit in the northern margin of the North China Craton, China. *Ore Geol. Rev.* **2020**, *125*, 103692. [CrossRef]
59. Lv, Z.H.; Chen, J.; Zhang, H.; Tang, Y. Petrogenesis of Neoproterozoic rare metal granite-pegmatite suite in Jiangnan Orogen and its implications for rare metal mineralization of peraluminous rock in South China. *Ore Geol. Rev.* **2020**, *128*, 103923. [CrossRef]
60. Lumpkin, G.R.; Ewing, R.C. Geochemical alteration of pyrochlore group minerals: Pyrochlore subgroup. *Am. Mineral.* **1995**, *80*, 732–743. [CrossRef]
61. Christy, A.G.; Atencio, D. Clarification of status of species in the pyrochlore supergroup. *Mineral. Mag.* **2013**, *77*, 13–20. [CrossRef]
62. Hogarth, D.D.; Williams, C.T.; Jones, P. Primary zoning in pyrochlore group minerals from carbonatites. *Mineral. Mag.* **2000**, *64*, 683–697. [CrossRef]
63. Hogarth, D.D. Classification and nomenclature of the pyrochlore group. *Am. Mineral.* **1977**, *62*, 403–410.
64. Wang, Y.R.; Li, J.T.; Lu, J.L.; Fan, W.L. Geochemical mechanism of Nb-, Ta-mineralization during the late stage of granite crystallization. *Geochemistry* **1982**, *1*, 175–185.
65. Nasraoui, M.; Bilal, E. Pyrochlores from the Lueshe carbonatite complex (Democratic Republic of Congo): A geochemical record of different alteration stages. *J. Asian Earth Sci.* **2000**, *18*, 237–251. [CrossRef]
66. Williams, C.T.; Wall, F.; Woolley, A.R.; Phillipo, S. Compositional variation in pyrochlore from the Bingo carbonatite, Zaire. *J. Afr. Earth Sci.* **1997**, *25*, 137–145. [CrossRef]
67. Bonazzi, P.; Bindi, L.; Zoppi, M.; Capitani, G.C.; Olmi, F. Single-crystal diffraction and transmission electron microscopy studies of "silicified" pyrochlore from Narssârssuk, Julianehaab district, Greenland. *Am. Mineral.* **2006**, *91*, 794–801. [CrossRef]
68. Bakker, J.; Elburg, M.A. A magmatic-hydrothermal transition in Arkaroola (northern Flinders Ranges, South Australia): From diopside–titanite pegmatites to hematite–quartz growth. *Contrib. Mineral. Petrol.* **2006**, *152*, 541–569. [CrossRef]
69. Jago, B.C.; Gittins, J. Pyrochlore crystallization in carbonatites: The role of fluorine. *S. Afr. J. Geol.* **1993**, *96*, 149–160.
70. Mitchell, R.H.; Kjarsgaard, B.A. Solubility of niobium in the system $CaCO_3$–$Ca(OH)_2$–$NaNbO_3$ at 0.1 GPa pressure. *Contrib. Mineral. Petrol.* **2002**, *144*, 93–97. [CrossRef]
71. Simons, B.; Andersen, J.C.Ø.; Shail, R.K.; Jenner, F.E. Fractionation of Li, Be, Ga, Nb, Ta, In, Sn, Sb, W and Bi in the peraluminous early permian Variscan granites of the Cornubian Batholith: Precursor processes to magmatic-hydrothermal mineralisation. *Lithos* **2017**, *278*, 491–512. [CrossRef]
72. Barsanov, G.P.; Yeremin, N.I.; Sergeyeva, N.Y.E. Columbite-tantalite zoning as revealed by electron-probe microanalysis. *Dokl. Akad. Nauk SSSR* **1971**, *201*, 174–176.

73. Norton, D.I.; Dutrow, B.L. Complex behavior of magma-hydrothermal processes: Role of supercritical fluid. *Geochim. Cosmochim. Acta* **2001**, *65*, 4009–4017. [CrossRef]
74. Zaraisky, G.P.; Korzhinskaya, V.; Kotova, N. Experimental studies of Ta_2O_5 and columbite–tantalite solubility in fluoride solutions from 300 to 550 °C and 50 to 100 MPa. *Mineral. Petrol.* **2010**, *9*, 287–300. [CrossRef]
75. Knudsen, C. Pyrochlore group minerals from the Qaqarssuk carbonatite complex. In *Lanthanides, Tantalum and Niobium*; Möller, P.Č.P., Saupé, F., Eds.; Springer: Berlin/Heidelberg, Germany, 1989; pp. 80–99.
76. Kjarsgaard, B.A.; Mitchell, R.H. Solubility of Ta in the system $CaCO_3$–$Ca(OH)_2$–$NaTaO_3$–$NaNbO_3$ ± F at 0.1 GPa: Implications for the crystallization of pyrochlore-group minerals in carbonatites. *Can. Mineral.* **2008**, *46*, 981–990. [CrossRef]
77. Mitchell, R.H.; Kjarsgaard, B.A. Solubility of niobium in the system $CaCO_3$–CaF_2–$NaNbO_3$ at 0.1 GPa pressure: Implications for the crystallization of pyrochlore from carbonatite magma. *Contrib. Mineral. Petrol.* **2004**, *148*, 281–287. [CrossRef]
78. Stepanov AMavrogenes, J.A.; Meffre, S.; Davidson, P. The key role of mica during igneous concentration of tantalum. *Contrib. Mineral. Petrol.* **2014**, *167*, 1009. [CrossRef]
79. Wang, R.C. Study on pyrochlore–group minerals from the Beauvoir granite, France. *Acta Petrol. Mineral.* **1994**, *2*, 140–148.
80. Xiong, X.L.; Zhao, Z.H.; Zhu, J.C.; Rao, B.; Lai, M.Y. Partitioning of F between aqueous fluids and albite granite melt and its petrogenetic and metallogenetic significance. *Chin. J. Geochem.* **1998**, *17*, 303–310.
81. Lin, Y.; Pollard, P.J.; Hu, S.Y.; Taylor, R.G. Geologic and geochemical characteristics of the Yichun Ta-Nb-Li deposit, Jiangxi Province, South China. *Econ. Geol.* **1995**, *90*, 577–585. [CrossRef]
82. Wang, W.Y.; Yang, Y.Q.; Chen, C.H.; Zhu, J.H. Study on the Nb and Ta–minerals from the granitic pegmatites in Nanping, Fujian Province. *Geol. Fujian* **1999**, *2*, 22.
83. Keppler, H. Influence of fluorine on the enrichment of high field strength trace elements in granitic rocks. *Contrib. Mineral. Petrol.* **1993**, *114*, 479–488. [CrossRef]
84. Mikhailova, J.A.; Pakhomovsky, Y.A.; Ivanyuk, G.Y.; Bazai, A.V.; Yakovenchuk, V.N.; Elizarova, I.R.; Kalashnikov, A.O. REE mineralogy and geochemistry of the Western Keivy peralkaline granite massif, Kola Peninsula, Russia. *Ore Geol. Rev.* **2017**, *82*, 181–197. [CrossRef]
85. Feng, S.Z. Geological characteristic and ore genesis of rare metal and rare-earth ore deposit in Baerze alkalic granite, Inner Mongolia. *Volcanol. Miner. Resour.* **2000**, *21*, 137–142.